denaturation at 95°C for 15 s, annealing at 58°C for 5 s, and extension at 72°C for 6 s. The lower detection limit of this assay is 1,000 copies.

Immunohistochemical Staining for HBV Core Antigen

For immunohistochemical staining of the HBV core antigen (HBcAg), mouse livers were fixed with 4% paraformaldehyde overnight, cryoprotected in 30% sucrose, and sectioned at a thickness of 10 μm using Leica cryostat and mounted on Superfrost glass slides. Sections were incubated with the primary antibody (anticore polyclonal rabbit antibody, DAKO) overnight, followed by incubation with an immunoperoxidase technique involving avidin-biotin peroxidase complexes (Vectastain ABC kit; Vector Laboratories, Burlingame, Calif., USA) according to a method reported previously [22].

HBV Surface Antigen Antigenemia

Mice were bled on the days mentioned after injection of pTER-1.4xHBV and serum was isolated by centrifugation. Concentration of HBV surface antigen (HBsAg) in the serum was quantified by sandwich ELISA in commercial ELISA kits following the manufacturer's protocol (XpressBio, USA). The reporting unit is the signal/cutoff ratio of the 1,000-fold diluted serum at an O.D. of 450 nm.

Southern Blotting to Detect Intracapsid HBV DNA

Viral DNA was isolated from intracellular viral capsids and detected with a specific DIG-labeled probe as described previously [21]. In brief, to isolate the viral DNA, mouse livers were homogenized and subjected to overnight sodium dodecyl sulfate-proteinase K digestion followed by phenol extraction and ethanol precipitation. Twenty micrograms of the isolated DNA was separated in 1% agarose gel, transferred onto Immobilon-Ny+ charged nylon membrane (Milipore), and detected with a full-length HBV-DNA probe labeled by the DIG DNA labeling and detection kit (Roche Diagnostics, Basel, Switzerland) according to the instructions provided by the manufacturer.

Anti-HBs Antibody ELISA

IgG antibodies specific for HBsAg were detected by ELISA as described previously [23] with slight modification. A 96-well plate was coated with antigen of HBs in carbonate buffer and followed by blocking of 2% BSA. Plasma samples were diluted 5× and then incubated in the antigen-coated wells for 3 h at room temperature. A horseradish peroxidase-conjugated goat anti-mouse IgGγ (Southern Biotechnology, USA) and TMB were used to develop the signal. Plates were read at 450 nm. Normal mouse plasma was used to generate cutoff values. The antibody titers are reported as the reciprocal of A_{450} (sample)/A_{450} (2.1' normal mouse average) at which samples with a value >1 were considered to have scored positive.

Quantitative HBV or Cytokines mRNA in the Organs

Each organ was extracted from the mice on the days mentioned after hydrodynamic injection of the HBV plasmid. Total RNA of the organs was isolated with TRIzol according to the manufacturer's protocol. Using 0.5–1 μg of total RNA as a template, cDNA was obtained using a high-capacity cDNA transcription kit (Applied Biosystems) according to manufacturer's instructions. qPCR was performed using a Step One real-time PCR system (Applied Biosystems). The expression of cytokine mRNA was normalized to that of β-actin mRNA in each organ, and the fold increase was determined by dividing the expression in each sample by that of the mice receiving the control plasmid. The primer sequences are described in online supplementary table 1.

Quantitative cGAS, STING, and MAVS Expression in Cell Lines

Total RNA was isolated from L929 cells, RAW264.7 cells, immortalized mouse hepatocytes, Huh7 cells, and HepG2 cells with TRIzol according to the manufacturer's protocol. Using 0.5–1 μg of total RNA as a template, cDNA was obtained using a high-capacity cDNA transcription kit (Applied Biosystems) according to manufacturer's instruction. qPCR was performed using a Step One real-time PCR system (Applied Biosystems). The expression of each targeted mRNA was normalized to that of β-actin mRNA in each sample and shown as a relative expression. The primer sequences are described in online supplementary table S1.

Reporter Gene Assay

To prepare the HBV RNA, immortalized mouse hepatocytes previously established in our laboratory [24] were transfected with either control plasmid or pTER1.4xHBV. Total RNA containing the HBV RNA was isolated after 12 h and confirmed with RT-PCR, while the RNA transfected with only control plasmid was used as a control. The isolated RNA was later used as stimuli for the reporter gene assay of IFN-β. Briefly, the immortalized hepatocytes were again transfected with the reporter plasmids. After 16 h, the immortalized hepatocytes were transfected with the stimuli including PIC, a control plasmid, HBV RNA, and pTER1.4xHBV using FuGENE HD (Roche). Cells were lysed at the time point mentioned using a passive lysis buffer, and Firefly and Renilla luciferase activities were determined using a dual-luciferase reporter assay kit. Firefly luciferase activity was normalized by Renilla luciferase activity and was expressed as the fold stimulation relative to activity in nonstimulated cells.

Statistical Analysis

The statistical significance of the obtained data in this study was analyzed using a two-tail unpaired t test and $p < 0.05$ was regarded as statistically significant.

Results

MAVS and TICAM-1 Are Dispensable in Suppressing HBV Replication

We hydrodynamically transfected replication-competent HBV DNA into *Mavs*$^{-/-}$ or *Ticam-1*$^{-/-}$ and *Mavs*$^{-/-}$/*Ticam-1*$^{-/-}$ mice to access the role of these viral RNA-sensing pathways in response to HBV. Serum HBsAg and HBV-DNA levels were monitored regularly as surrogate markers of HBV replication in vivo. WT mice displayed acute self-limiting hepatitis with peak HBs antigenemia on day 4 after DNA injection (fig. 1a–c). Subsequently, HBsAg in sera decreased and terminated by day 11. *Mavs*$^{-/-}$ and *Ticam-1*$^{-/-}$ mice displayed HBsAg clearance

Downloaded by:
Hokkaido Daigaku
133.87.71.181 - 12/25/2015 5:04:42 AM

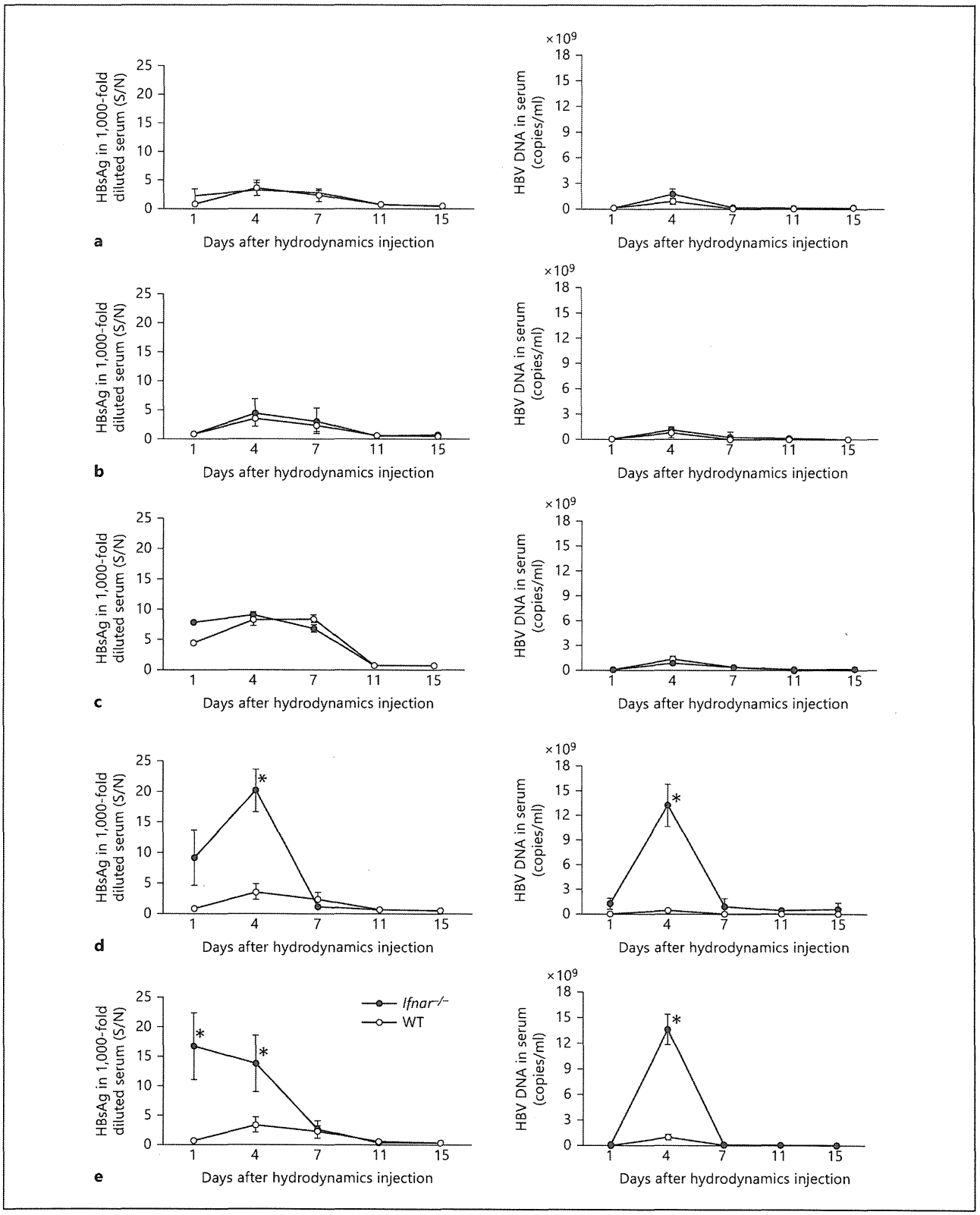

1

(*For legend see next page.*)

J Innate Immun 2015;7:47–58
DOI: 10.1159/000365113

Downloaded by:
Hokkaido Daigaku
133.87.71.151 - 12/25/2014 5:04:42 AM

kinetics that closely paralleled the WT mice response (fig. 1a, b, left panels). Serum HBV-DNA levels were quantified using real-time PCR. The average titer of serum HBV DNA in 15 WT mice injected with HBV DNA was below 1×10^4 copies/ml 1 day after injection and reached 2×10^9 copies/ml 4 days after injection (fig. 1a–c, right panels). At later time points, most mice showed no detectable virus titer. Similar results were obtained with *Mavs*$^{-/-}$ and *Ticam-1*$^{-/-}$ mice (fig. 1a, b). The serum HBV-DNA and HBsAg results showed only a marginal effect for the absence of MAVS or TICAM-1 compared to WT mice. The results suggested that the pathways involving these two adaptor proteins were dispensable for triggering the immune responses that suppressed HBV replication.

To determine whether the RIG-I/MDA5-MAVS and TLR3-TICAM-1 RNA-sensing pathways were dispensable for suppressing the HBV replication, similar studies were performed in mice lacking both the MAVS and TICAM-1 adaptor proteins (fig. 1c). No notable differences were observed between WT and MAVS/TICAM-1 double-knockout mice in serum HBsAg and HBV-DNA levels, consistent with other data obtained. In addition, similar kinetics of intrahepatic clearance of the HBV template as well as HBV replication was observed in WT, *Mavs*$^{-/-}$, and *Ticam-1*$^{-/-}$ mice as revealed by Southern blotting using HBV-specific probes (online suppl. fig. 1).

To ensure the efficiency of delivery of the HBV transcriptional template into the mouse liver, a plasmid harboring the *lacZ* gene was used to transfect the liver cells using the hydrodynamic injection method. X-gal (a substrate for *lacZ*) staining showed that nearly the entire liver of injected mice has successfully received the injected plasmid (online suppl. fig. 2). An independent determination of transfection efficiency was carried out using a plasmid harboring the GFP fragment. The comparable transfection efficiencies observed did not differ significantly among the different mouse strains (data not shown). Furthermore, quantification of HBV mRNA in the organs of WT and knockout mice on day 3 after hydrodynamic injection revealed that HBV mRNA was amplified mainly in the liver but not in other organs, including kidney, lung, heart, spleen, and thymus (online suppl. fig. 3). Only weak HBV signals were detected in other organs in some types of knockout mice. These results demonstrated that HBV replication in vivo using the injection method was efficient and liver specific.

To further assess the possibility of HBV RNA acting as pathogen-associated molecular patterns to trigger the induction of type I IFN in hepatocytes, we transfected the immortalized hepatocytes with a plasmid containing the full genome of HBV as well as RNA containing the HBV mRNA. Along with the synthetic analog of dsRNA, poly(I:C), as a control, we determined the activity of the IFN-β promoter upon the stimulation using reporter gene assay (online suppl. fig. 4). Unlike poly(I:C), neither the full genome of HBV nor RNA induced any activity of the type I IFN promoter in the immortalized hepatocytes. Furthermore, we quantified the endogenous expression of genes including *cGas*, *Sting*, and *Mavs* in the hepatocyte cell lines in order to access the intrinsic RNA or DNA-sensing pathways (online suppl. fig. 5). We found that the hepatocyte cell lines, including those originating from mice and humans, expressed extremely low amounts of *Sting* compared to the intrinsic *Mavs*. However, other cell lines, including RAW 264.7 (murine macrophage cell line) and L929 (murine fibrosarcoma cell line), have higher endogenous expression of *Sting* in comparison to *Mavs*.

IRF-3/IRF-7 and IFNAR Are Critical Factors for HBV Replication Regulation

To investigate the mechanisms underlying the rapid termination of HBV replication in WT mice, we examined HBV clearance in IRF-3-/IRF-7-deficient mice. Activation of transcription factors including IRF-3 or IRF-7 is essential for raising immune responses including IFN production [25]. Unlike *Mavs*$^{-/-}$, *Ticam-1*$^{-/-}$, or WT mice, mice lacking the transcription factors IRF-3/IRF-7 had

Fig. 1. IFNAR and IRF-3/IRF-7 are critically associated with regulation of HBV propagation in mice but not MAVS and/or TICAM-1. HBsAg or HBV DNA were measured with sera from *Mavs*$^{-/-}$ (n = 13) (**a**), *Ticam-1*$^{-/-}$ (n = 10) (**b**), *Ticam-1*$^{-/-}$/*Mavs*$^{-/-}$ (n = 6) (**c**), *Irf-3*$^{-/-}$/*Irf-7*$^{-/-}$ (n = 12) (**d**), and *Ifnar*$^{-/-}$ (n = 13) (**e**) mice compared to WT mice (n = 15). These mice were hydrodynamically injected with 50 μg of the pTER-1.4xHBV plasmid containing full-genome HBV DNA. Mouse sera were isolated at the time points indicated. The HBsAg titers in the 1,000-fold diluted serum (left) and HBV DNA (right) in the knockout mice (●) were compared to the WT mice (○). Serum HBsAg titers were determined with an enzyme immunoassay at O.D. 450 nm [calculated as signal-over-noise ratios (S/N)]. Sera HBV DNA were determined by Q-PCR and indicated as copies per milliliter. Error bars indicate SD. The statistical p values were analyzed and no significant differences were observed in **a–c**. * $p < 0.01$ in **d** and **e** are time points statistically different between WT and transgenic mice.

Downloaded by:
Hokkaido University
153.67.71.151 - 12/25/2014 6:04:42 AM

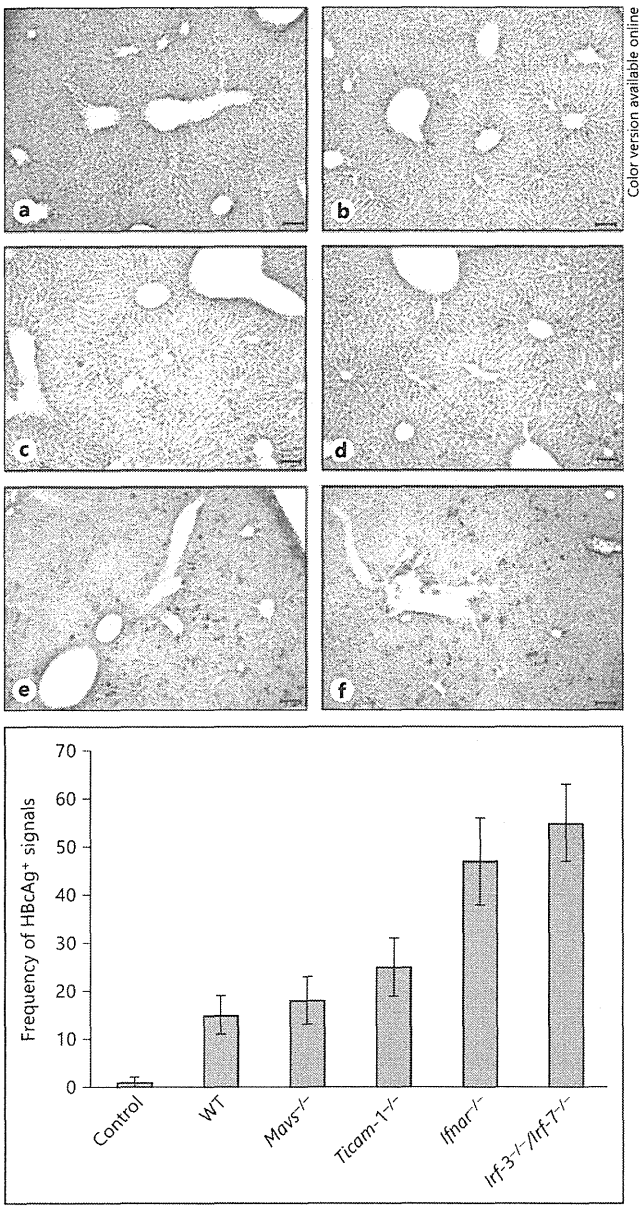

Fig. 2. Lacking IFNAR and IRF-3/IRF-7 causes an increase of HBcAg in mouse liver injected with the HBV replicative plasmid. The HBc protein in the livers on day 3 after injection was visualized with immunohistochemical staining of the mice liver sections embedded in OCT using an anti-HBc antibody for HBcAg. Representative sections are shown. HBcAg-positive cells were absent in the WT mice that received only the control plasmid (**a**). Only marginal differences were observed in the frequency of HBcAg-positive cells between WT (**b**), *Mavs*$^{-/-}$ (**c**), and *TICAM-1*$^{-/-}$ (**d**) mice. Frequency of HBcAg-positive cells in the livers of the *Ifnar*$^{-/-}$ (**e**) and *Irf-3*$^{-/-}$/*Irf-7*$^{-/-}$ (**f**) mice are more prevalent compared to the WT mice. The scale bars represent 10 μm. The images are displayed at 200× magnification. Frequency of HBcAg-positive signals between the different mouse strains shown is based on 3 images of each.

markedly high amounts of HBsAg and HBV DNA in sera (fig. 1d). A sharp peak of HBsAg in sera occurred in *Irf-3*$^{-/-}$/*Irf-7*$^{-/-}$ mice on day 4 after injection. However, in spite of the high virus titer at the early stage, HBsAg and DNA in sera were cleared with kinetics that paralleled the WT mice response, and viremia was eliminated by day 11. Hence, the substantial differences in the serum viremia between WT and *Irf-3*$^{-/-}$/*Irf-7*$^{-/-}$ mice in the early stage after transfection presumably reflects the importance of the genes being expressed with these transcription factors in the suppression of the HBV replication. IRF-3 and IRF-7 are the key molecules in the suppression of HBV viremia in the early stage after HBV injection.

Since type I IFN stimulates the IFNAR pathway to amplify type I IFN production, we hydrodynamically transfected HBV plasmid into mice lacking the gene of the type I IFN receptor (*Ifnar*$^{-/-}$) and assessed the suppression of HBV replication. *Ifnar*$^{-/-}$ mice showed markedly high titers of viral DNA and antigens in sera (fig. 1e) similar to *Irf-3*$^{-/-}$/*Irf-7*$^{-/-}$ mice.

The presence of HBcAg-positive hepatocytes was also monitored by immunohistochemical staining of liver sections from mice of each strain at day 4 after the injections (fig. 2). Data from the observed HBcAg-positive hepatocytes were in good agreement with the results on sera HBsAg and HBV DNA: only deficiency of IRF-3/IRF-7 and IFNAR resulted in a sharp increase of viremia in mice in the early stage (earlier than day 4). Fewer HBcAg-positive hepatocytes were observed in *Mavs*$^{-/-}$ and *Ticam1*$^{-/-}$ as well as WT mice at day 4 after injection than in *Irf-3*$^{-/-}$/*Irf-7*$^{-/-}$ or *Ifnar*$^{-/-}$ mice (fig. 2).

To gain insight into cytokine production in the liver in response to the HBV genome and its replication, we quantified the expression of type I IFN, IFN-γ, IL-7, IL-12p40, and chemokines including CXCL9, CXCL10, and CXCL11 mRNA in the livers of WT mice receiving either the control plasmid or plasmid carrying the HBV full genome on days 1, 3, 7, and 10 after hydrodynamic injection. Replication of HBV in the liver did not cause any significant changes in the expression of the cytokines or chemokines except the IFNs and CXCL-10 (fig. 3a–h). A similar study was carried out in WT and *Ifnar*$^{-/-}$ mice in order to further elaborate the type I IFN production. The IFNs increased in WT mice livers receiving the HBV full genome compared to the mouse livers receiving the control plasmid (fig. 3i–k). This increase was not observed in *Ifnar*$^{-/-}$ mice lacking the INF receptor. Although there appeared to be slight individual-to-individual differences in the apparent peaks of IFN-α induction, the result indicated that IFN-β was responsible for suppressing HBV

Downloaded by:
Hokkaido Daigaku
133.87.71.161 - 12/25/2014 5:04:42 AM

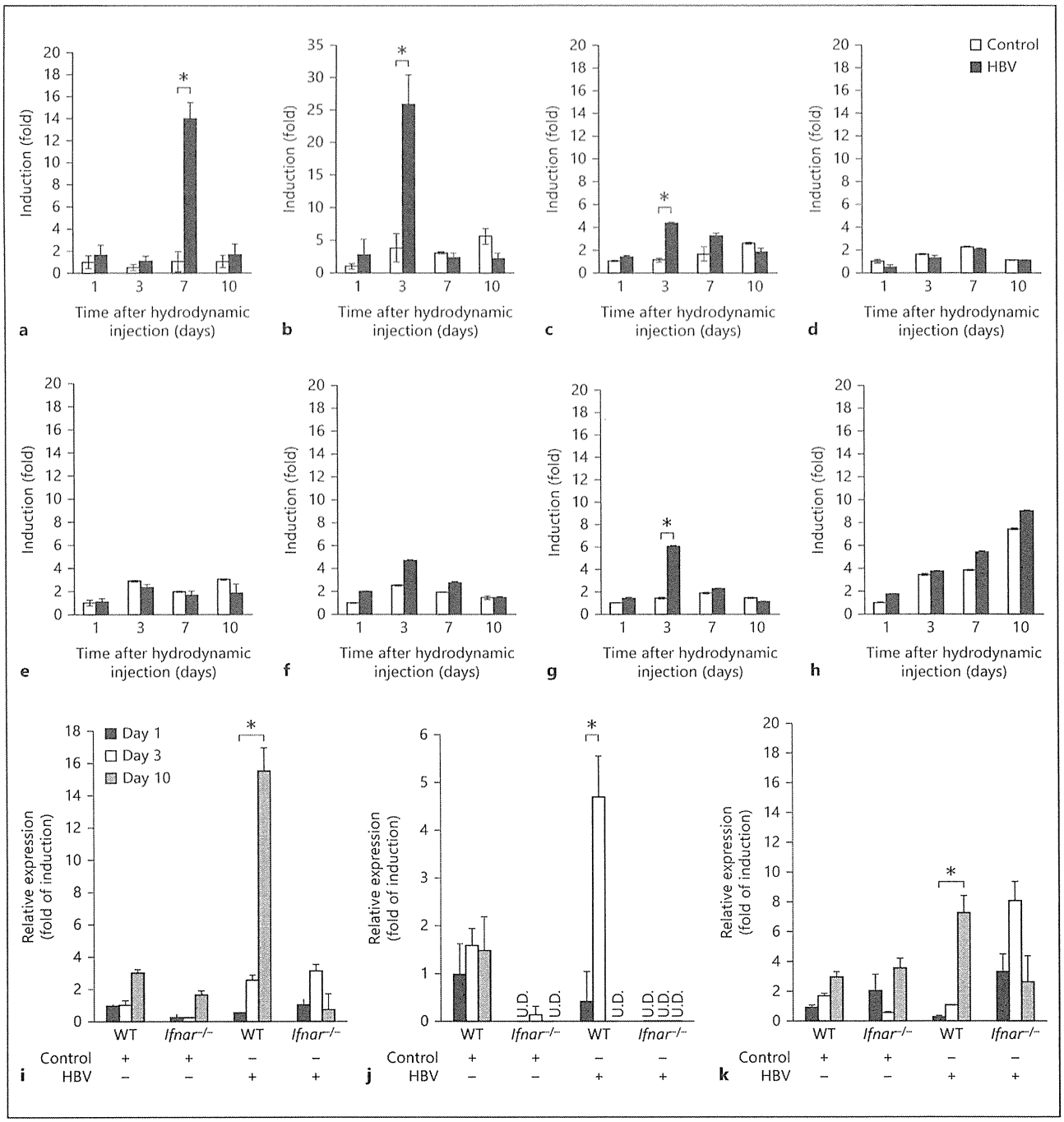

Fig. 3. Type I and II IFN expression is induced by HBV replication, and lacking the type I IFN receptor (IFNAR) causes failure of these inductions. WT mice were hydrodynamically injected with 50 μg of the pTER-1.4xHBV or control plasmid as described, and livers were isolated on days 1, 3, 7, and 10 after injection. The expression of IFN-α (**a**), IFN-β (**b**), IFN-γ (**c**), IL-7 (**d**), IL-12p40 (**e**), CXCL-9 (**f**), CXCL-10 (**g**), and CXCL-11 (**h**) mRNA was determined by reverse transcription followed by real-time PCR, and was expressed as the fold of induction relative to the WT mice receiving the control plasmid. Induction of IFNs and CXCL-10 was observed in the mice receiving the HBV plasmid. Similar studies were conducted in the WT and *Ifnar*$^{-/-}$ mice: IFN-α (**i**), IFN-β (**j**), and IFN-γ (**k**). *Ifnar*$^{-/-}$ mice show reduced expression of the IFNs compared to the WT. Data represent the mean of 3 mice on each strain and time point mentioned. * $p < 0.05$. U.D. = Undetected.

Downloaded by:
Hokkaido Daigaku
133.87.71.181 - 12/25/2021 8:04:42 AM

replication early. However, the reason for the lag in the induction of IFN-γ between the WT and *Ifnar*$^{-/-}$ mice remains unclear.

Taken together, these results suggest that type I IFN was indispensable for suppressing HBV replication in the early stage after viral genome entry. Type I IFN binds to its receptor to induce intracellular antiviral proteins to disrupt HBV replication. The results, however, infer that intrahepatic HBV clearance at the later stage is independent of IFN.

HBV Clearance in a Later Stage by Acquired Immunity

Previous studies by Yang et al. [23] and other groups showed that HBV replication persists indefinitely in globally immunodeficient mice such as NOD/Scid mice hydrodynamically injected with the replication-competent plasmid carrying the full genome of HBV. To investigate whether the elevated viral titer in *Ifnar*$^{-/-}$ and *Irf-3*$^{-/-}$/*Irf-7*$^{-/-}$ mice on day 4 after hydrodynamic injection and intrahepatic HBV clearance were related to immune effectors including T and B cells, HBV clearance was examined in *Rag-2*$^{-/-}$ mice. The lack of V(D)J recombination in this strain resulted in failure to produce mature B or T lymphocytes. As shown in figure 4, the absence of mature T and B cells in the *Rag-2*$^{-/-}$ mice did not result in elevated viral titer immediately after transfection, unlike in *Ifnar*$^{-/-}$ and *Irf-3*$^{-/-}$/*Irf-7*$^{-/-}$ mice. However, *Rag-2*$^{-/-}$ mice failed to clear the input plasmid and HBV products, as sera HBsAg and HBV DNA were detected up to day 15 (fig. 4a), by the time viral replication was terminated in all the other strains tested (fig. 4c, d). In other words, activation of the immune effectors such as the B and T cells is responsible for the intrahepatic HBV clearance, their activation being independent of IFN and IRF-3/IRF-7.

MyD88 Deficiency Leads to Slower HBV Clearance

The MyD88-dependent pathway has been known to lead to the production of inflammatory cytokines and is common to all TLRs, except TLR3 [22]. To examine whether a MyD88-dependent pathway is required in the intrahepatic clearance of the HBV, we monitored the serum HBsAg in MyD88-deficient mice. As shown in figure 4b, an increase in sera HBsAg in *Myd88*$^{-/-}$ mice was observed, although without particular antigenemia peaks at the early stage of transfection in *Ifnar*$^{-/-}$ and *Irf-3*$^{-/-}$/*Irf-7*$^{-/-}$ mice (fig. 4b, c). Instead, a delay in the elimination of the HBV was observed (fig. 4b, d). Typically, WT mice or other mouse strains lose serum HBsAg from day 11 after injection. However, serum antigen was detectable on day 15 in *Myd88*$^{-/-}$ mice. Delayed elimination of HBV plasmid and single-strand DNA in the liver was observed in Southern analysis of the liver from *Myd88*$^{-/-}$ mice compared with WT, *Mavs*$^{-/-}$, and *Ticam-1*$^{-/-}$ mice (online suppl. fig. 1).

Additionally, ELISA to determine anti-HBsAg antibody production in mouse sera after hydrodynamic injection revealed that anti-HBs antibody was produced in WT mice from day 7 and peaked at day 15 (fig. 4e). RAG2-deficient mice lacking mature T and B cells failed to produce any antibody, and *Myd88*$^{-/-}$ mice also had lower or nearly undetectable anti-HBs antibody in serum in comparison to the typical response of WT mice at later transfection stages. These results suggested that MyD88 and RAG2 were crucial for triggering acquired immunity against HBV in vivo.

Discussion

In the present study, several different knockout mice were analyzed in an attempt to define the mechanism of innate immunity against HBV in vivo. The evidence we obtained indicated that viral replication was not affected by MAVS or TICAM-1 knockout, but absence of IRF-3 or IRF-7 transcription factors, as well as the IFN receptor, had an adverse effect on the inhibition of HBV replication. The results herein demonstrated that the TICAM-1 and MAVS pathways were not required in either suppressing the virus replication or intrahepatic clearance of HBV replicative plasmid in vivo.

Although a DNA virus, HBV has the unique feature of replicating via an RNA proviral intermediate that is copied into DNA. Thus, defining the virus component, either HBV DNA or RNA that triggers the antiviral response is crucial to understand the immune mechanisms that are responsible for eliminating HBV during infection. HBV RNA has been suggested as the putative pathogen-associated molecular pattern of HBV in a few reports [16–18, 26]. HBx or HBs inhibits IFN-β induction followed by activation of TLR3 or RIG-I pathways with poly(I:C) or SeV, respectively. However, these findings must be interpreted with caution, as poly(I:C) and SeV are heterologous inducers for evaluating either the TLR3 or RIG-I pathway [16, 17]. No definitive conclusion on activation of the TLR3 or RIG-I pathway by HBV RNA in vivo has been reported yet.

Viral RNA is recognized largely by RIG-I or MDA5 in the cytosol of infected cells [27, 28] and by TLR3 or

Downloaded by:
Hokkaido Daigaku
133.87.71.181 - 12/29/2014 8:04:42 AM

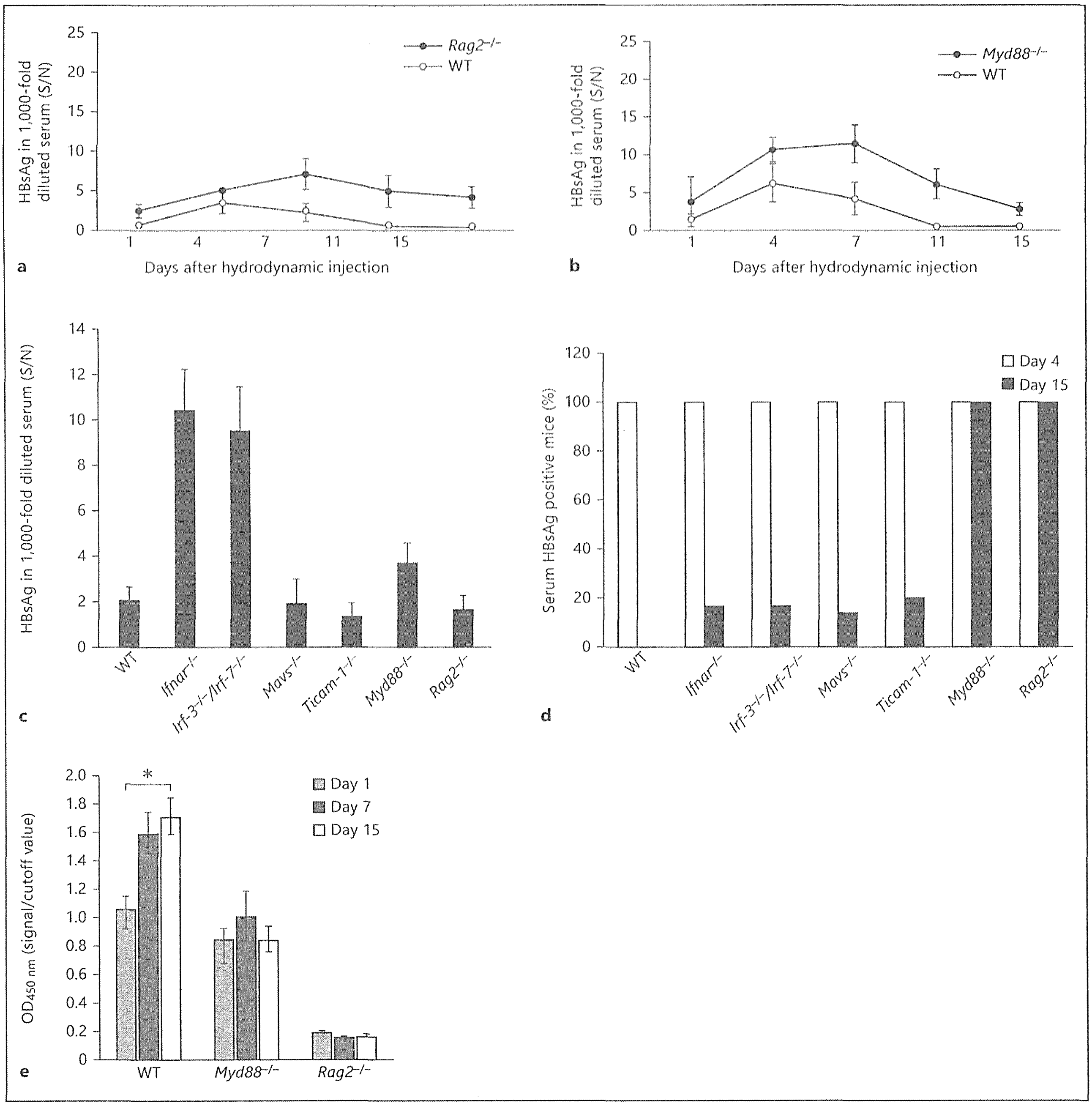

Fig. 4. Mice lacking RAG2 and MyD88 show insufficient clearance of HBV. **a, b** The *Rag2*$^{-/-}$, *Myd88*$^{-/-}$, and WT mice were hydrodynamically injected with 50 μg of pTER-1.4xHBV and HBsAg in the mouse sera at the time points indicated and analyzed with ELISA as described. **c** HBsAg in 1,000-fold diluted serum from all the mice strains including WT, *Ifnar*$^{-/-}$, *Irf-3*$^{-/-}$/*Irf-7*$^{-/-}$, *Mavs*$^{-/-}$, *Ticam-1*$^{-/-}$, *Myd88*$^{-/-}$, and *Rag2*$^{-/-}$ at day 4 after the hydrodynamic injections. Only *Ifnar*$^{-/-}$ and *Irf-3*$^{-/-}$/*Irf-7*$^{-/-}$ mice show a remarkable increase, while a moderate increase of sera HBsAg was seen in *Myd88*$^{-/-}$ mice. **d** HBsAg persistence rates in all the mice strains receiving pTER1.4HBV were determined by the percentage of serum HBsAg-positive mice on day 4 (□) and day 15 (■) after the hydrodynamic injections. Serum HBsAg was found to be persistent only in mice deficient in MyD88 and RAG2 on day 15 as 100% of the mice from these two strains were HBsAg positive (n = 8 for each mice strain). **e** Lacking MyD88 and RAG2 leads to the failure of the knockout mice to produce anti-HBs IgG compared to the WT mice on day 15 after injection as determined by ELISA using antigen of HBs (n = 3 for each mice strain). * $p < 0.05$. S/N = Signal-over-noise ratio.

Downloaded by:
Hokkaido Daigaku
133.87.71.151 - 12/25/2014 8:04:42 AM

TLR7/8 in the endosome of other noninfected cells [29, 30]. These RNA sensors require MAVS, TICAM-1, or MyD88 as adaptor proteins to induce type I IFN [28]. On the other hand, cytoplasmic DNA is recognized by DNA sensors including DAI, IFI16, RIG-I, DHX9 (helicase), and cGAS [31]. STING is the only adaptor for all IFN-inducing DNA sensors in mouse cells reported so far [30, 32, 33], although some of these sensors are reported to induce type I IFN via MAVS in human cells. These adaptors, TICAM-1, MAVS, and STING, are all linked to activation of IRF-3/IRF-7 which act as transcription factors that induce activation of the type I IFN promoter during viral infections. Involvement of different pathways in the induction of type I IFN is critically dependent on the virus species and cell type. Cell type-specific contributions of other sensors, including DEAD box helicases, might occur in some cases of infection. However, in hepatocytes, the control plasmid per se exhibited no IFN-inducing response, suggesting that the HBV replication is a critical step for IFN induction. Actually, no contribution of other sensors except RIG-I/MDA5 and TLR3 has been reported so far.

Using the murine hydrodynamic injection model, we found that mice deficient in IRF-3 and IRF-7 or IFNAR do not inhibit HBV replication as effectively as their WT counterparts and result in elevated HBV titers in mice sera and livers. These findings imply that type I IFN acting on IFNAR is indispensable for evoking anti-HBV protective responses although such a hypothesis is in disagreement with previous findings that HBV does not induce detectable changes in type I IFN expression during the early weeks of infection [34]. There are a few possibilities of how type I IFN is produced in mice receiving HBV template plasmid. One of them is that HBV could be recognized by pathways that do not link to MAVS or TICAM-1 and facilitate IFN production in the cytoplasm. For instance, STING-dependent signaling leads to type I IFN induction, and it has been shown that this can be MAVS and TICAM-1 independent. Notably, STING-dependent signaling is especially associated with DNA-mediated induction of type I IFN via IRF-3/IRF-7, and genomic DNA is an important part of HBV replication. It would be interesting to clarify such hypotheses using *Sting*$^{-/-}$ mice in the near future.

To elucidate the molecular pattern which triggers type I IFN induction, we transfected either HBV DNA or RNA into immortalized hepatocytes. To our surprise, we were unable to detect significant IFN-β induction with either HBV replicative DNA or HBV RNA. As we looked into the possible reasons to account for the lack of innate immune responses against HBV in hepatocytes, we found that the endogenous expression of STING in hepatocyte cell lines including HepG2 and immortalized mouse hepatocytes is extremely low compared to other cell lines like macrophages or dendritic cells, thus suggesting that STING-dependent signaling might play a crucial role in inducing type I IFN in response to HBV. The produced IFN in turn activates the IFNAR pathway. There are various cells populations in the liver that express IFNAR and therefore subsequently initiate a natural signaling cascade for amplification of IFN production via the Jak-STAT pathway.

Another possible way for HBV to induce IFN is via the HBV-stimulated nonparenchymal or resident myeloid cells. Even though there has been no report suggesting that HBV substantially infects pDCs, Isogawa et al. [5], demonstrated that freshly isolated CD11c^{+} cells of intrahepatic myeloid cells rather than the hepatocytes expressed TLRs including TLR2, 3, and 9. Therefore, resident myeloid cells might induce IFN to further prevent the spread of HBV by activating the IFNAR pathway in bystander cells or hepatocytes.

Although *Myd88*$^{-/-}$ mice receiving an HBV-DNA injection did not exhibit significantly high virus titers in the early phase unlike those observed in *Ifnar*$^{-/-}$ and *Irf-3*$^{-/-}$/*Irf-7*$^{-/-}$ mice, interestingly MyD88 is required for the intrahepatic clearance of the HBV replicative template. The fact that the transcriptional template persists in the absence of MyD88 suggests that MyD88 may play a pivotal role in intrahepatic HBV clearance in the mouse model. Notably, MyD88 is the adaptor molecule for TLR7 and 9 in pDCs [35, 36]. Deficiency of MyD88 in pDCs may result in failure to induce acquired immunity for HBV. Our findings show that HBV-specific antibodies are efficiently produced in WT, but not in *Myd88*$^{-/-}$ mice. In addition, the number of pDCs has been previously reported to be reduced in vivo during several systemic viral infections including HBV [37]. In one of the most recent reports, Lv et al. [38], showed that HBV-derived CpG induces potent IFN-α production by human pDCs, which may partially explain how pDCs interact with HBV in infection. However, the cause of weak participation in the early response of IFN induction in *Myd88*$^{-/-}$ mice remains to be determined.

Recombinant IFN-α is a standard treatment for chronic HBV patients. Nevertheless, direct treatment with IFN yields only about 30% improvement in HBV patients and little is known about why most chronic HBV patients do not respond to IFN therapy [39]. As demonstrated in our study, virus persistency can be independent of the type I

Downloaded by:
Hokkaido Daigaku
133.87.71.151 - 12/25/2015 8:04:42 AM

IFN-inducing system. This observation leads to the suggestion that type I IFN is indispensable for inducing antiviral molecules to control viral replication and spread before the onset of more specific and powerful adaptive immune responses. This appeared to be factual at least in our knockout mouse models as virus titers were highly elevated in *Ifnar*$^{-/-}$ mice in the initial days after injection. Conversely, type I IFN did not have any influential effects on clearance of the HBV template in the later stages. Such observations coincide with the latest study conducted in patients with chronic HBV infection by Tan et al. [40], in which IFN-α treatment was shown to modulate innate immune parameters in the patients, but without any detectable effect on HBV-specific adaptive immunity. The missing link between the induction of type I IFN and anti-HBV cellular effectors needs to be further investigated in mouse models, including the mechanism of MyD88 participation in activation of the cellular immune response during infection. Elucidating molecular mechanisms between innate pattern sensing and evoking cellular effectors may provide a reasonable explanation for the failure of IFN-treatment in HBV infection.

Collectively, our study validates the use of the hydrodynamic transfection method in mimicking acute HBV infection in mouse models and demonstrated the host-virus relationship during HBV infection in many aspects. Since HBV infectious models with immunologically well-defined laboratory animals do not exist, the result presented in this study herein provides an insight into the dispensability of RNA sensors for induction of IFN by HBV RNA and the complexity of innate and adaptive immunity during HBV clearance.

Acknowledgements

This work was supported in part by Grants-in-Aid from the Ministry of Education, Science, and Culture and the Ministry of Health, Labor, and Welfare of Japan, and the Yasuda Cancer Foundation (T.S.) and the Ono Foundation (T.S.). Financial support by a MEXT Grant-in-Project 'The Carcinogenic Spiral', 'The National Cancer Center Research and Development Fund (23-A-44)', and the Japan Initiative for Global Research Network on Infectious Diseases (J-GRID) are gratefully acknowledged. We are grateful to Drs. H. Shime, J. Kasamatsu, K. Funami, and M. Tatematsu in our laboratory for their fruitful discussions. We thank Dr. F.V. Chisari (Scripps Research Institute, La Jolla, Calif., USA) for providing us with HBV plasmid and sleeping beauty.

Disclosure Statement

The authors declare no financial or commercial conflict of interest.

References

1 Guidotti LG, Chisari FV: Immunobiology and pathogenesis of viral hepatitis. Annu Rev Pathol 2006;1:23–61.
2 Zuckerman JN, Zuckerman AJ: Current topics in hepatitis B. J Infect 2000;41:130–136.
3 Ganem D, Prince AM: Hepatitis B virus infection – natural history and clinical consequences. N Engl J Med 2004;350:1118–1129.
4 Seeger C, Mason WS: Hepatitis B virus biology. Microbiol Mol Biol Rev 2000;64:51–68.
5 Isogawa M, Robek MD, Furuichi Y, Chisari FV: Toll-like receptor signaling inhibits hepatitis B virus replication in vivo. J Virol 2005;79:7269–7272.
6 Wu J, Lu M, Meng Z, Trippler M, Broering R, Szczeponek A, Krux F, Dittmer U, Roggendorf M, Gerken G, Schlaak JF: Toll-like receptor-mediated control of HBV replication by nonparenchymal liver cells in mice. Hepatology 2007;46:1769–1778.
7 Kawai T, Takahashi K, Sato S, Coban C, Kumar H, Kato H, Ishii KJ, Takeuchi O, Akira S: IPS-1, an adaptor triggering RIG-I- and Mda5-mediated type I interferon induction. Nat Immunol 2005;6:981–988.
8 Akira S, Uematsu S, Takeuchi O: Pathogen recognition and innate immunity. Cell 2006;124:783–801.
9 Takeuchi O, Akira S: Innate immunity to virus infection. Immunol Rev 2009;227:75–86.
10 Oshiumi H, Matsumoto M, Funami K, Akazawa T, Seya T: TICAM-1, an adaptor molecule that participates in Toll-like receptor 3-mediated interferon-β induction. Nat Immunol 2003;4:161–167.
11 Ishikawa H, Ma Z, Barber GN: STING regulates intracellular DNA-mediated, type I interferon-dependent innate immunity. Nature 2009;461:788–792.
12 Cheng G: Double-stranded DNA and double-stranded RNA induce a common antiviral signaling pathway in human cells. Proc Natl Acad Sci USA 2007;104:9035–9040.
13 Ablasser A, Bauernfeind F, Hartmann G, Latz E, Fitzgerald KA, Hornung V: RIG-I-dependent sensing of poly(dA:dT) through the induction of an RNA polymerase III-transcribed RNA intermediate. Nat Immunol 2009;10:1065–1072.
14 Chiu YH, Macmillan JB, Chen ZJ: RNA polymerase III detects cytosolic DNA and induces type I interferons through the RIG-I pathway. Cell 2009;138:576–591.
15 Stetson DB, Medzhitov R: Type I interferons in host defense. Immunity 2006;25:373–381.
16 Kumar M, Jung SY, Hodgson AJ, Madden CR, Qin J, Slagle BL: Hepatitis B virus regulatory HBx protein binds to adaptor protein IPS-1 and inhibits the activation of beta interferon. J Virol 2011;85:987–995.
17 Wei C, Ni C, Song T, Liu Y, Yang X, Zheng Z, Jia Y, Yuan Y, Guan K, Xu Y, Cheng X, Zhang Y, Wang Y, Wen C, Wu Q, Shi W, Zhong H: The hepatitis B virus X protein disrupts innate immunity by down regulating mitochondrial antiviral signaling protein. J Immunol 2010;185:1158–1168.
18 Yu S, Chen J, Wu M, Chen H, Kato N, Yuan Z: Hepatitis B virus polymerase inhibits RIG-I- and Toll-like receptor 3-mediated beta interferon induction in human hepatocytes through interference with interferon regulatory factor 3 activation and dampening of the interaction between TBK1/IKKepsilon and DDX3. J Gen Virol 2010;91:2080–2090.
19 Oshiumi H, Okamoto M, Fujii K, Kawanishi T, Matsumoto M, Koike S, Seya T: The TLR3/TICAM-1 pathway is mandatory for innate immune responses to poliovirus infection. J Immunol 2011;187:5320–5327.

Downloaded by:
Hokkaido Daigaku
133.87.71.161 - 12/29/2014 8:04:42 AM

20 Akazawa T, Ebihara T, Okuno M, Okuda Y, Shingai M, Tsujimura K, Takahashi T, Ikawa M, Okabe M, Inoue N, et al: Antitumor NK activation induced by the Toll-like receptor 3-TICAM-1 (TRIF) pathway in myeloid dendritic cells. Proc Natl Acad Sci USA 2007;104: 252–257.
21 Noguchi C, Ishino H, Tsuge M, Fujimoto Y, Imamura M, Takahashi S, Chayama K: G to A hypermutation of hepatitis B virus. Hepatology 2005;41:626–633.
22 Tian Y, Chen WL, Kuo CF, Ou JH: Viral-load-dependent effects of liver injury and regeneration on hepatitis B virus replication in mice. J Virol 2012;86:9599–9605.
23 Yang PL, Althage A, Chung J, Chisari FV: Hydrodynamic injection of viral DNA: a mouse model of acute hepatitis B virus infection. Proc Natl Acad Sci USA 2002;99:13825–13830.
24 Aly HH, Oshiumi H, Shime H, Matsumoto M, Wakita T, Shimotohno K, Seya T: Development of mouse hepatocyte lines permissive for hepatitis C virus (HCV). PLoS One 2011; 6:e21284.
25 Honda K, Taniguchi T: IRFs: master regulators of signalling by Toll-like receptors and cytosolic pattern-recognition receptors. Nat Rev Immunol 2006;6:644–658.
26 Wang X, Li Y, Mao A, Li C, Tien P: Hepatitis B virus X protein suppresses virus-triggered IRF3 activation and IFN-beta induction by disrupting the VISA-associated complex. Cell Mol Immunol 2010;7:341–348.
27 Kawai T, Akira S: Innate immune recognition of viral infection. Nat Immunol 2006;7:131–137.
28 Onomoto K, Yoneyama M, Fujita T: Regulation of antiviral innate immune responses by RIG-I family of RNA helicases. Curr Top Microbiol Immunol 2007;316:193–205.
29 Matsumoto M, Oshiumi H, Seya T: Antiviral responses induced by the TLR3 pathway. Rev Med Virol 2011, DOI: 10.1002/rmv.680.
30 Diebold SS: Recognition of viral single-stranded RNA by Toll-like receptors. Adv Drug Deliv Rev 2008;60:813–823.
31 Paludan SR, Bowie AG: Immune sensing of DNA. Immunity 2013;38:870–880.
32 Ishikawa H, Barber GN: The STING pathway and regulation of innate immune signaling in response to DNA pathogens. Cell Mol Life Sci 2011;68:1157–1165.
33 Suzuki T, Oshiumi H, Miyashita M, Aly HH, Matsumoto M, Seya T: Cell type-specific subcellular localization of phospho-TBK1 in response to cytoplasmic viral DNA. PLoS One 2013;8:e83639.
34 Bertoletti A, Gehring AJ: The immune response during hepatitis B virus infection. J Gen Virol 2006;87:1439–1449.
35 Hoshino K, Sasaki I, Sugiyama T, Yano T, Yamazaki C, Yasui T, Kikutani H, Kaisho T: Critical role of IkappaB Kinase alpha in TLR7/9-induced type I IFN production by conventional dendritic cells. J Immunol 2010; 184:3341–3345.
36 Hoshino K, Sugiyama T, Matsumoto M, Tanaka T, Saito M, Hemmi H, Ohara O, Akira S, Kaisho T: IkappaB kinase-alpha is critical for interferon-alpha production induced by Toll-like receptors 7 and 9. Nature 2006;440: 949–953.
37 Swiecki M, Wang Y, Vermi W, Gilfillan S, Schreiber RD, Colonna M: Type I interferon negatively controls plasmacytoid dendritic cell numbers in vivo. J Exp Med 2011;208: 2367–2374.
38 Lv S, Wang J, Dou S, Yang X, Ni X, Sun R, Tian Z, Wei H: Nanoparticles encapsulating HBV-CpG induce therapeutic immunity against hepatitis B virus infection. Hepatology 2014;59:385–394.
39 Ter Borg MJ, Hansen BE, Bigot G, Haagmans BL, Janssen HL: ALT and viral load decline during PEG-IFN alpha-2b treatment for HBeAg-positive chronic hepatitis B. J Clin Virol 2008;42:160–164.
40 Tan AT, Hoang LT, Chin D, Rasmussen E, Lopatin U, Hart S, Bitter H, Chu T, Gruenbaum L, Ravindran P, Zhong H, Gane E, Lim SG, Chow WC, Chen PJ, Petric R, Bertoletti A, Hibberd ML: Reduction of HBV replication prolongs the early immunological response to IFNα therapy. J Hepatol 2014;60: 54–61.

Downloaded by:
Hokkaido University
133.87.71.181 - 12/25/2014 5:04:42 AM

INAM Plays a Critical Role in IFN-γ Production by NK Cells Interacting with Polyinosinic-Polycytidylic Acid–Stimulated Accessory Cells

Jun Kasamatsu,* Masahiro Azuma,*,[1] Hiroyuki Oshiumi,* Yuka Morioka,[†] Masaru Okabe,[‡] Takashi Ebihara,*,[2] Misako Matsumoto,* and Tsukasa Seya*

Polyinosinic-polycytidylic acid strongly promotes the antitumor activity of NK cells via TLR3/Toll/IL-1R domain–containing adaptor molecule 1 and melanoma differentiation-associated protein-5/mitochondrial antiviral signaling protein pathways. Polyinosinic-polycytidylic acid acts on accessory cells such as dendritic cells (DCs) and macrophages (Mφs) to secondarily activate NK cells. In a previous study in this context, we identified a novel NK-activating molecule, named IFN regulatory factor 3–dependent NK-activating molecule (INAM), a tetraspanin-like membrane glycoprotein (also called Fam26F). In the current study, we generated INAM-deficient mice and investigated the in vivo function of INAM. We found that cytotoxicity against NK cell–sensitive tumor cell lines was barely decreased in *Inam*$^{-/-}$ mice, whereas the number of IFN-γ–producing cells was markedly decreased in the early phase. Notably, deficiency of INAM in NK and accessory cells, such as CD8α$^+$ conventional DCs and Mφs, led to a robust decrease in IFN-γ production. In conformity with this phenotype, INAM effectively suppressed lung metastasis of B16F10 melanoma cells, which is controlled by NK1.1$^+$ cells and IFN-γ. These results suggest that INAM plays a critical role in NK-CD8α$^+$ conventional DC (and Mφ) interaction leading to IFN-γ production from NK cells in vivo. INAM could therefore be a novel target molecule for cancer immunotherapy against IFN-γ–suppressible metastasis. *The Journal of Immunology*, **2014, 193: 5199–5207.**

Microbial components play a major role in activating innate and adaptive immune responses by triggering pattern recognition receptors. Nucleic acid adjuvants, including polyinosinic-polycytidylic acid (polyI:C) and unmethylated CpG dinucleotides, strongly promote Th1 immune responses against cancer and infected cells and induce type I IFN and other inflammatory cytokines (1, 2). PolyI:C strongly enhances priming and expansion of Ag-specific T cells and NK cells with dramatic regression of syngeneic implant tumors in mice (3–6). NK cells belong to group 1 innate lymphocytes (ILC1s) and control progression of several types of tumors and microbial infections (7). Although polyI:C (an analog of viral dsRNA) is a ligand for multiple receptors, including dsRNA-dependent protein kinase, retinoic acid–inducible gene-I, melanoma differentiation–associated protein-5 (MDA5), and TLR3, both of the pathways initiated by TLR3/Toll/IL-1R domain–containing adaptor molecule 1 (TICAM-1) and MDA5/mitochondrial antiviral signaling protein confer antitumor activity on NK cells in vivo (8, 9).

PolyI:C also directly and indirectly activates human NK cells and other ILC1s (10, 11). PolyI:C participates in secondary activation of murine NK cells through stimulation of accessory cells such as dendritic cells (DCs) and other myeloid cells (12–14). In these interactions, previous studies have shown that type I IFN and cell contact via IL-15 receptors play a critical role in accessory cell activation followed by NK activation (15). In contrast, our previous studies showed that polyI:C induced bone marrow–derived DC (BMDC)–mediated NK cell activation through the TLR3/TICAM-1/IFN regulatory factor 3 (IRF3) pathway, which promoted antitumor immunity by adoptive transfer in a type I IFN- and IL-15–independent manner (8, 16). As the key molecule for this NK–DC interaction, we identified a novel IRF3-inducible tetraspanin-like membrane glycoprotein, named IRF3-dependent NK-activating molecule (INAM). INAM expression was induced not only in myeloid DCs but also in NK cells by polyI:C stimulation in vivo. Transfection of INAM in both BMDC and NK cells cooperated in inducing IFN-γ production and cytotoxicity against the NK-sensitive B16D8 cell line.

To investigate the role of INAM in vivo, we generated INAM-deficient mice by the standard gene-targeting method. INAM expression was induced not only in NK cells and conventional DC

*Department of Microbiology and Immunology, Graduate School of Medicine, Hokkaido University, Sapporo 060-8638, Japan; [†]Division of Disease Model Innovation, Institute for Genetic Medicine, Hokkaido University, Sapporo 060-8638, Japan; [‡]Research Institute for Microbial Disease, Osaka University, Osaka 565-0871, Japan

[1]Current address: Department of Pathology and Cellular Biology, Faculty of Medicine, University of Montreal, Montreal, QC, Canada.

[2]Current address: Department of Medicine, Howard Hughes Medical Institute, Washington University School of Medicine, St. Louis, MO.

Received for publication April 11, 2014. Accepted for publication September 9, 2014.

This work was supported in part by grants-in-aid from the Ministry of Education, Culture, Sports, Science and Technology and the Ministry of Health, Labor and Welfare of Japan, a Ministry of Education, Culture, Sports, Science and Technology of Japan Grant-in-Aid Project for Basic Research, "Carcinogenic Spiral," and the National Cancer Center Research and Development Fund (23-A-44). This work was also supported by the Takeda Science Foundation, the Yasuda Cancer Research Foundation, and the Iskra Foundation. J.K. is a Research Fellow of the Japan Society for the Promotion of Science.

Address correspondence and reprint requests to Prof. Tsukasa Seya, Department of Microbiology and Immunology, Graduate School of Medicine, Hokkaido University, Kita 15, Nishi 7, Kita-ku, Sapporo 060-8638, Japan. E-mail address: seya-tu@pop.med.hokudai.ac.jp

The online version of this article contains supplemental material.

Abbreviations used in this article: BMDC, bone marrow–derived DC; BST2, bone marrow stromal cell Ag 2; cDC, conventional DC; DC, dendritic cell; IFNAR1, IFN (α and β) receptor 1; ILC1, group 1 innate lymphocyte; INAM, IFN regulatory factor 3–dependent NK-activating molecule; IRF, IFN regulatory factor; Mφ, macrophage; MDA5, melanoma differentiation–associated protein-5; pDC, plasmacytoid DC; polyI:C, polyinosinic-polycytidylic acid; qPCR, quantitative real-time PCR; TICAM-1, Toll/IL-1R domain–containing adaptor molecule 1; WT, wild-type.

Copyright © 2014 by The American Association of Immunologists, Inc. 0022-1767/14/$16.00

www.jimmunol.org/cgi/doi/10.4049/jimmunol.1400924

Downloaded from http://www.jimmunol.org/ at Hokkaido University on February 15, 2015

(cDC) subsets but also in other immune cells including macrophages (Mφs) and plasmacytoid DCs (pDCs) by polyI:C stimulation. Cytotoxicity against NK cell–sensitive tumor cell lines was barely decreased in *Inam*$^{-/-}$ mice, whereas the number of IFN-γ–producing cells markedly decreased in the early phase. We also showed that CD8α$^+$ cDCs and Mφs facilitate secretion of IFN-γ from NK cells in response to polyI:C stimulation in vitro and in vivo. Notably, deficiency of INAM on NK and their accessory cells led to a robust decrease in IFN-γ production. Therefore, these results infer that INAM plays a critical role in the interaction of NK-CD8α$^+$ cDCs (and Mφs) leading to IFN-γ production from NK cells. In agreement with this suggested phenotype, INAM effectively suppressed lung metastasis of B16F10 melanoma cells by controlling activation of NK1.1$^+$ cells and IFN-γ. Taken together, these results provide the first demonstration, to our knowledge, that INAM plays a critical role in the interaction of NK–CD8α$^+$ cDCs, which allows NK cells to produce IFN-γ. We propose in this study that INAM is a novel target molecule for immunotherapy against IFN-γ–suppressible tumors.

Materials and Methods

Mice

All mice were backcrossed with C57BL/6 mice more than seven times before use. A C57BL/6 background *Inam* (*Fam26f*)–targeted embryonic stem cell line, JM8A3.N1 of FAM26F tm2a (European Conditional Mouse Mutagenesis Program) Wtsi, was purchased from the European Conditional Mouse Mutagenesis Program. Chimeric mice were generated by aggregation of the mutated embryonic stem cells at the 8 cell stage. To remove exon 2 of *Inam*, the *Inam* heterozygous mutants were crossed with Cre-transgenic mice. The *Inam* heterozygous mutants obtained were intercrossed to obtain *Inam* homozygous mutants. *Ticam-1*$^{-/-}$ and *Mavs*$^{-/-}$ mice were generated in our laboratory (8, 16). *Irf-3*$^{-/-}$ and *Ifnar1*$^{-/-}$ mice were provided by Dr. T. Taniguchi (17). *Batf3*$^{-/-}$ C57BL/6 mice were purchased from The Jackson Laboratory (Bar Harbor, ME) (18). The *Batf3*$^{-/-}$ mice of C57BL/6 background [unlike 129 and BALB/c background (19)] lacked splenic CD8a$^+$ DCs as described previously (18) and evoked insufficient T cell functional response against extrinsic Ag and adjuvant (Azuma et al., submitted for publication). C57BL/6 background were purchased from CLEA Japan (Shizuoka, Japan). Experiments were performed with sex-matched mice at 8–14 wk of age. All mice were bred and maintained under specific pathogen-free conditions in the animal facility of the Hokkaido University Graduate School of Medicine. Animal experimental protocols and guidelines were approved by the Animal Safety Center, Hokkaido University.

Semiquantitative RT-PCR and quantitative real-time PCR

Total RNA was extracted using TRIzol according to the manufacturer's instructions (Invitrogen). cDNA was generated by using the High Capacity cDNA Transcription Kit (ABI) with random primers according to the manufacturer's instructions. Quantitative real-time PCR (qPCR) was performed using the Step One Real-Time PCR system (ABI). The primer sequences for qPCR analysis were 5′-CAACTGCAATGCCACGCTA-3′ and 5′-TCCAACCGAACACCTGAGACT-3′ for *Inam*; 5′-TTAACTGAGGCTGGCATTCATG-3′ and 5′-ACCTACACTGACACAGCCCAAA-3′ for *Il15*; 5′-GACAAAGAAAGCCGCCTCAA-3′ and 5′-ATGGCAGCCATTGTTCCTG-3′ for *Il18*; 5′-ACCGTGTTTACGAGGAACCCTA-3′ and 5′-GGTGAGAGCTGGCTGTTGAG-3′ for *Irf7*; 5′-GCCGAGACACAGGCAAAC-3′ and 5′-CCAGGGCTTGAGACACCTTC-3′ for bone marrow stromal cell Ag 2 (*Bst2*); and 5′-GCCTGGAGAAACCTGCCA-3′ and 5′-CCCTCAGATGCCTGCTTCA-3′ for *Gapdh*. The primer sequences for semi-qPCR analysis were 5′-CAACTGCAATGCCACGCTA-3′ and 5′-TCCAACCGAACACCTGAGACT-3′ for *Gapdh*.

Mφ depletion and stimulation using TLR agonists in vivo

To generate Mφ-depleted mice, mice were injected i.p. with 150 μl Clophosome-Clodronate Liposomes (FormuMax). For qPCR analysis of *Inam* induction using some TLR antagonists in Fig. 1E, mice were injected i.p. with 50 μg polyI:C (GE Bioscience), 50 μg Pam3CSK4 (Boehringer Ingelheim), 10 μg LPS (Sigma-Aldrich), 50 μg R837 (InvivoGen), and 50 μg CpG ODN1826 (InvivoGen). In other experiments, polyI:C was injected i.p. at a dose of 200 μg/mouse.

Cells

For isolation of DC subsets, Mφs and NK cells, spleens were treated with 400 Mandle U/ml collagenase D (Roche) at 37°C for 25 min in HBSS (Sigma-Aldrich). EDTA was added, and the cell suspension was incubated for an additional 5 min at 37°C. NK cells were purified from spleens by positive selection of DX5-positive cells with DX5 MACS beads (Miltenyi Biotec). CD8α$^+$ cDCs were purified using a CD8α$^+$ DC isolation kit and CD11c MACS beads (Miltenyi Biotec). CD8α$^-$ cDCs were purified with CD11c MACS beads (Miltenyi Biotec) from the negative fraction after CD8α$^+$ cDC separation. F4/80$^+$ Mφs were isolated using MACS-positive selection beads (Miltenyi Biotec) as described previously (13). pDC Ag-1$^+$ pDCs were isolated with pDC Ag-1 MACS beads (Miltenyi Biotec). All immune cells were purified from spleens by repeated positive selection to achieve high purity (90%). Leukocytes from the lung were prepared as previously reported (18). Mouse immune cells were cultured in RPMI 1640/10% FCS/55 μM 2-ME/10 mM HEPES. B16D8, B16F10, YAC-1, and RMA-S were cultured in RPMI 1640/10% FCS.

Cell culture

To investigate potential interactions with NK–accessory cells, MACS-sorted accessory cells were cocultured with freshly isolated NK cells (accessory cells /NK = 1:2) with or without 20 μg/ml polyI:C for 24 h. In some coculture experiments using the transwell system, NK cells were added to 0.4-μm pore transwells (Corning) in the presence of polyI:C. Activation of NK cells was assessed by measuring the concentration of IFN-γ (ELISA; GE Healthcare) in the medium. For the IFN (α and β) receptor 1 (IFNAR1) blocking experiment, anti-IFNAR Ab at a final concentration of 10 μg/ml was added to the cultures before addition of polyI:C. For measurement of IL-12p40 and type I IFNs, we used ELISA kits purchased from BioLegend and PBL Biomedical Laboratories, respectively.

FACS analysis

For intracellular cytokine staining of NK cells, we isolated spleen or lung from polyI:C- or PBS-injected mice at each time point and harvested their leukocytes as described previously (18, 19). The leukocytes were incubated in medium with 10 μg/ml brefeldin A for 4 h. Cells were fixed and stained with a combination of anti-NK1.1 (PK136) and anti-CD3ε (145-2C11) Abs (BioLegend), followed by permeabilization and staining with anti-IFN-γ (XMG1.2) Ab (BioLegend), anti–granzyme B (NGZB) Ab (eBioscience), anti–TNF-α (MP6-XT22) Ab (BioLegend), anti–GM-CSF (MP1-22E9) Ab (BioLegend), or anti–IL-2 (JES6-5H4) Ab (BioLegend) using a BD Cytofix/Cytoperm Kit (BD Biosciences). For staining of the C terminus of INAM of each immune cell type, after treatment of anti-CD16/32 (no. 93), cell-surface molecules of splenocytes were stained with anti-CD3ε (145-2C11), anti-CD8α (53-6.7), anti-CD11c (N418), anti-NK1.1, anti-F4/80 (BM8), anti-Gr1 (RB6-8C5), anti-CD11b (M1/70), or anti-CD19 (MB19-1) Abs (BioLegend) or with anti-B220 (RA3-6B2) or anti-CD4 (L3T4) Abs (eBioscience). After staining of the cell surface, cells were fixed and permeabilized using a BD Cytofix/Cytoperm Kit (BD Biosciences) and then stained with an anti-INAM polyclonal Ab as described previously (16). To detect activating markers, NK receptors, and developmental markers, splenocytes were stained with anti-CD27 (LG.3A10), anti-CD25 (PC61), anti-NKp46 (29A1.4), anti-NKG2D (C7), anti-DNAM-1 (10E5), and anti-TRAIL (N2B2) Abs from BioLegend or anti-Fas (Jo2) from BD Biosciences. For detection of dead cells, samples were stained with ViaProbe from BD Biosciences. Samples were processed on an FACSCalibur flow cytometer and analyzed with FlowJo software (Tree Star).

Tumor inoculation and polyI:C treatment

PolyI:C therapy against mice with B16D8 tumor burden was described previously (8). B16F10 melanoma cells (2×10^5) were injected into wild-type (WT) or *Inam*$^{-/-}$ mice via the tail vein on day 0. PolyI:C was injected i.p. on days 1, 4, 7, and 10 at a dose of 200 μg/mouse. The control group was treated with PBS. All mice were killed 12 d after tumor inoculation. The lungs were excised and fixed in Mildform (Wako) for counting of surface colonies under a dissection microscope.

Statistical analysis

Statistical analyses were made with the Student *t* test for paired data. Statistical analyses were made with ANOVA in multiple comparisons. The *p* value of significant differences is reported.

Results

Generation of INAM-deficient mice

We designed a targeting vector to disrupt exon 2, which encodes the C-terminal transmembrane and cytoplasmic regions of INAM

Downloaded from http://www.jimmunol.org/ at Hokkaido University on February 15, 2015

(Fig. 1A). The heterozygosity and homozygosity of siblings were verified by Southern blot analysis (Fig. 1B). Mutant mice were born at the expected Mendelian ratio from *Inam*$^{-/-}$ and *Inam*$^{+/-}$ parents and showed normal healthy development under specific pathogen-free conditions (Fig. 1C). We also examined the composition of immune cells in the spleen and found no clear difference between WT and *Inam*$^{-/-}$ mice (Table I). Murine NK cells are divided into four subsets in their maturation stage based on the surface density of CD27 and CD11b: CD11b^{low}/CD27^{low}, CD11b^{low}/CD27^{high}, CD11b^{high}/CD27^{high}, and CD11b^{high} /CD27^{low} (20). We examined the composition of splenic NK cells in each maturation stage and found no clear difference between WT and *Inam*$^{-/-}$ mice (Supplemental Fig. 1A). A previous study showed that *Inam* mRNA is highly expressed in spleen and thymus under steady-state conditions

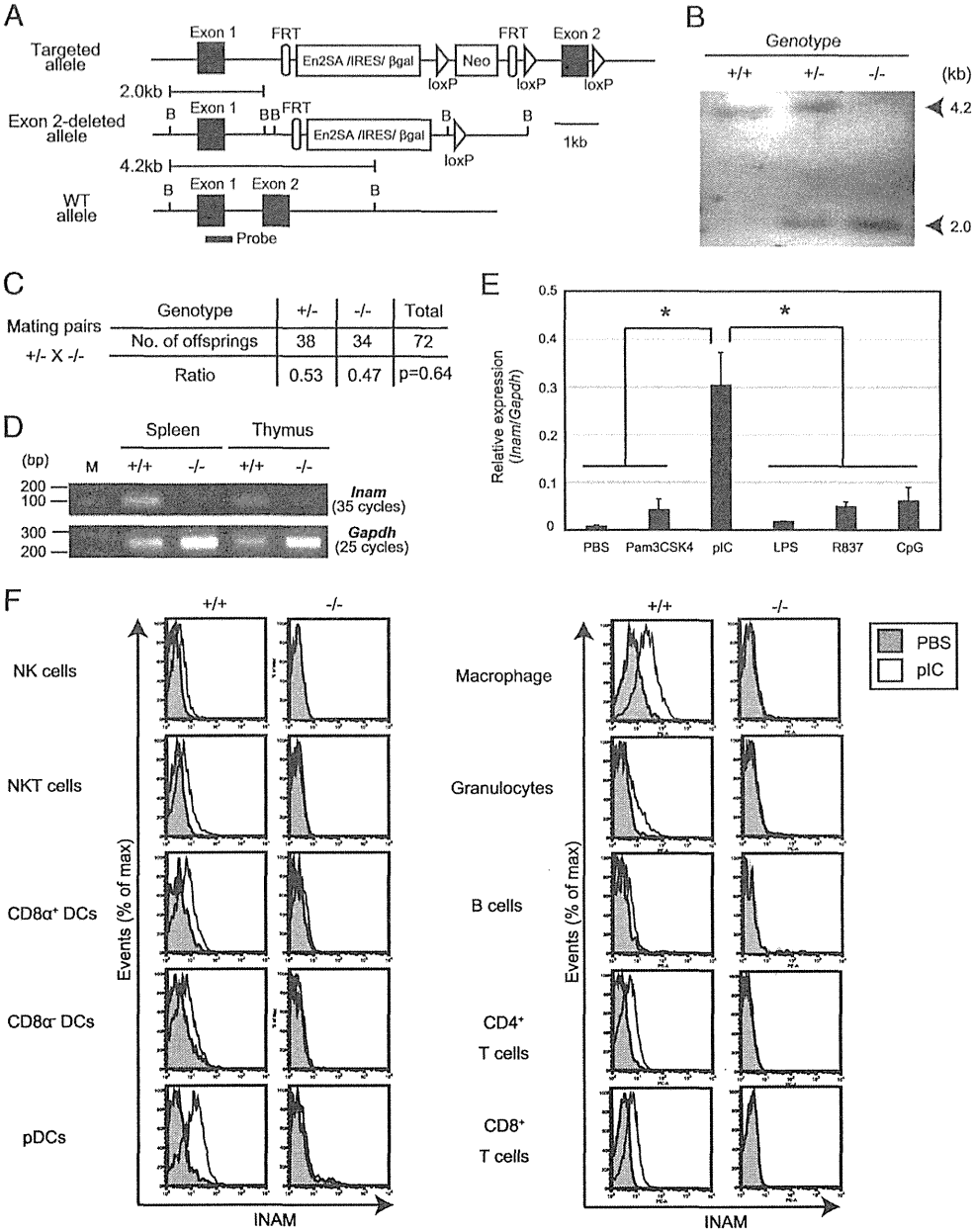

FIGURE 1. Generation of INAM-deficient mice. (**A**) Structure of the mouse *Inam*-targeted, *Inam*-disrupted, and WT allele. Closed boxes indicate the coding exon of Inam. A probe (602 bp) for Southern blot analysis was designed in exon 1. (**B**) Southern blot analysis of BamHI-digested genomic DNA isolated from WT (+/+), heterozygous mutant (+/−), and homozygous mutant (−/−) mice. (**C**) Genotype analyses of offspring from heterozygote intercrosses. The χ^2 goodness-of-fit test indicated that deviation from the Mendelian ratio was not statistically significant ($p > 0.1$). (**D**) RT-PCR analysis of spleen and thymus. Total RNA sets from spleen and thymus in WT (+/+) and *Inam*$^{-/-}$ (−/−) mice were extracted and subjected to RT-PCR to determine *Inam* expression. (**E**) *Inam* mRNA expression in response to TLR agonists. Total RNA were isolated from the spleens of mice in each group ($n = 3$) at 3 h after TLR agonist stimulation and subjected to quantitative PCR to determine to determine *Inam* expression. *$p < 0.05$ (**F**) INAM expression of immune cells. WT (+/+) and *Inam*$^{-/-}$ (−/−) mice were i.p. injected with 200 μg polyI:C (pIC) or PBS ($n = 2$). After 12 h, INAM expression of each immune cell type was analyzed by flow cytometry. Open histograms and shaded histograms indicate immune cells derived from the mice. Immune cells were classified as NK cells (CD3ε$^-$/NK1.1$^+$), NKT cells (CD3ε$^-$/NK1.1^{int}), B cells (CD19c$^+$/B220$^+$), CD8$^+$ T cells (CD3ε$^+$/CD8α$^+$), CD4$^+$ T cells (CD3ε$^+$/CD4α$^+$), classic CD8α$^-$ cDCs (CD11c^{high}/CD8α$^-$), classic CD8α$^+$ cDCs (CD11c^{high}/CD8α$^+$), pDCs (CD11c^{int}/B220$^+$), Mφs (CD11c$^{low\text{-}dim}$/CD11b$^{low\text{-}dim}$/F4/80$^+$), and granulocytes (CD11b^{high}/Gr-1$^+$). The data shown are representative of at least two independent experiments.

Downloaded from http://www.jimmunol.org/ at Hokkaido University on February 15, 2015

Table I. Development of hematopoietic cells in INAM-deficient mice

Cells	WT	*Inam*$^{-/-}$	Student *t* Test
CD4$^+$ T cells	16.9 ± 0.3	16.2 ± 2.2	$p = 0.69$
CD8$^+$ T cells	8.6 ± 0.5	8.0 ± 1.0	$p = 0.27$
B cells	55.6 ± 1.9	56.4 ± 3.5	$p = 0.65$
NK cells	1.2 ± 0.4	2.3 ± 0.7	$p = 0.22$
NKT cells	0.9 ± 0.1	0.76 ± 0.2	$p = 0.27$
pDCs	1.0 ± 0.1	1.0 ± 0.1	$p = 0.91$
CD8α$^+$ DCs	0.2 ± 0.01	0.3 ± 0.02	$p = 0.03$
CD8α$^-$ DCs	0.49 ± 0.03	0.8 ± 0.2	$p = 0.09$
Granulocytes	0.3 ± 0.04	1.0 ± 1.2	$p = 0.43$
Mφ	1.8 ± 0.6	2.2 ± 0.8	$p = 0.45$
Resident monocytes	0.4 ± 0.1	0.4 ± 0.1	$p = 0.96$
Inflammatory monocytes	0.2 ± 0.03	0.2 ± 0.2	$p = 0.82$

Data are percentages unless otherwise indicated.

(16). In our study, mRNA expression of *Inam* in these tissues was clearly absent in the *Inam*-null mouse (Fig. 1D). To assess the induction of *Inam* mRNA expression in response to TLR agonists in vivo, we performed qPCR analysis using spleens at 3 h after i.p. administration of those agonists or PBS. The levels of *Inam* mRNA expression was strongly induced by polyI:C, but not other TLR agonists (Fig. 1E). Hence, these data indicate that polyI:C is the strongest TLR agonist to induce *Inam* expression of the TLR agonists tested in vivo. To investigate the cellular distribution of INAM protein expression, we performed flow cytometric analysis using polyclonal Abs to mouse INAM after i.p. administration of polyI:C. The levels of INAM protein expression in these cells clearly reflected the absence of the mRNA (Fig. 1F). Flow cytometric analysis of spleen cells demonstrated that INAM expression was induced in all myeloid lineage cells, including DC subsets and NK cells. In particular, INAM expression was highly induced in pDCs and F4/80$^+$ Mφs.

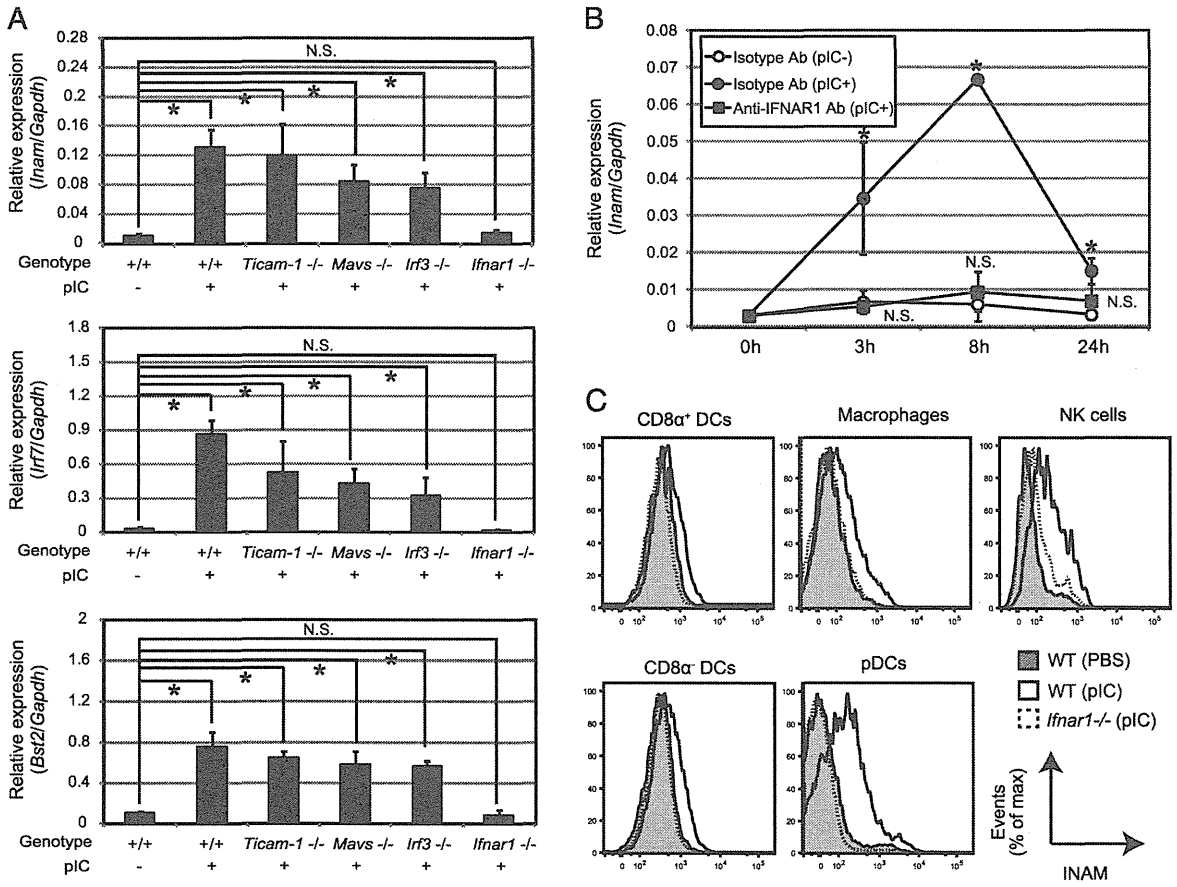

FIGURE 2. Signaling pathway of INAM induction in vivo. (**A**) *Inam* expression in splenocytes derived from various gene-manipulated mice. After 3 h, total RNA were isolated from the spleens of mice in each group ($n = 3$) and subjected to quantitative PCR to determine *Inam*, *Irf7*, and *Bst2* expression. (**B**) Type I IFN signaling is required for *Inam* expression of splenocytes derived from WT mice. Splenocytes ($n = 3$) were treated with polyI:C (pIC), IFNAR1-blocking Ab, or isotype control Ab for 0, 3, 8, and 24 h. (**C**) Type I IFN signaling is required for INAM expression of DC subsets, NK cells, and Mφs. WT and *Ifnar1*$^{-/-}$ mice were i.p. injected with 200 μg polyI:C or PBS ($n = 2$). After 12 h, INAM expression of each immune cell type was analyzed by flow cytometry. The data shown are representative of at least two independent experiments. Data are means ± SD of three independent samples. *$p < 0.05$.

Downloaded from http://www.jimmunol.org/ at Hokkaido University on February 15, 2015

Type I IFN signaling is required for INAM induction in vivo

The TLR3/TICAM-1 and MDA5/mitochondrial antiviral signaling protein pathways activate the transcription factor IRF3 in response to viral RNA. In BMDC, polyI:C (an analog of virus dsRNA) directly induces INAM expression via the TICAM-1/IRF3 pathway (16). Moreover, in the absence of pattern recognition receptor signals, IFN-α stimulation triggers INAM expression in BMDC. However, it is unclear which innate signal is required for its up-regulation in vivo. To understand the inducible pathway of *Inam* expression, we investigated its expression in spleen cells derived from various genetically manipulated mice. After polyI:C stimulation, *Inam* expression was completely undetectable in IFN (α and β) receptor 1 (*Ifnar1*)$^{-/-}$ mice, but not in *Ticam-1*$^{-/-}$ mice, a similar pattern of expression to that seen in type I IFN–inducible genes including *Irf7* and *Bst2* (Fig. 2A). Additionally, *Inam* expression was partially reduced in mice deficient in *Mavs* or *Irf3*, factors that are critical for producing type I IFN in response to polyI:C (3, 16). To assess the effect of type I IFN in WT mice, splenocytes were stimulated with polyI:C in the presence of anti-IFNAR1 Ab or isotype control Ab. Expression of *Inam* was transient, peaking at 8 h in the stimulated group in the presence of isotype control Ab (Fig. 2B). In contrast, blocking of the type I IFN receptor led to abrogation of *Inam* induction. In agreement with these results, INAM protein expression was completely undetectable in DC subsets, NK cells, and Mφs derived from IFNAR1-deficient mice (Fig. 2C). Hence, these data indicate that INAM expression depends on the IFNAR1 signaling pathway in vivo.

INAM is required for IFN-γ production through NK–accessory interaction

To identify the accessory cells directly responding to polyI:C and leading to IFN-γ production from NK cells, we performed an experiment on a coculture consisting of MACS-sorted splenic NK cells and myeloid immune cells including DC subsets and Mφs. Purified NK cells cultured in medium with or without polyI:C did not produce IFN-γ (Fig. 3A). In contrast, a high level of IFN-γ production was observed in the supernatant of NK cells cocultured with CD8α$^+$ cDCs and Mφs in the presence of polyI:C, but not in pDCs and CD8α$^-$ cDCs. In our reports, cell-to-cell contact is required for the interaction between NK cells and BMDC (8, 16). To confirm that the cell-to-cell contact is a prerequisite for the interaction between NK cells and splenic accessory cells, we performed coculture experiments using transwell system. As

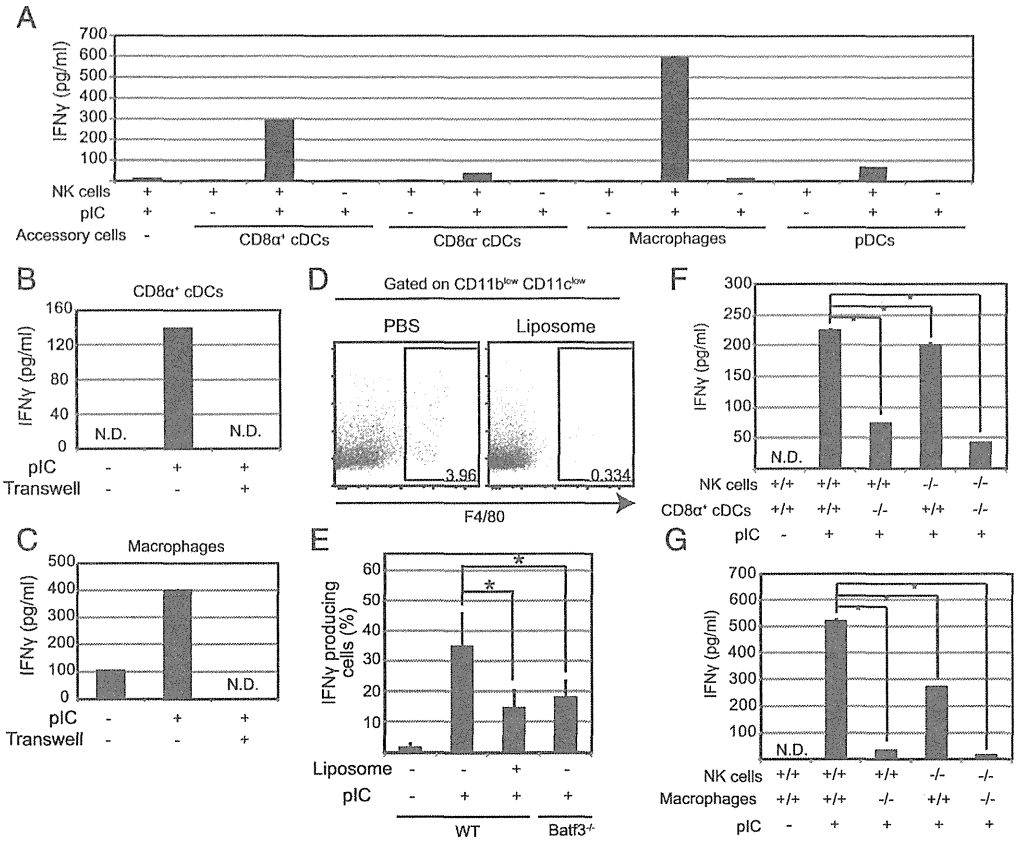

FIGURE 3. INAM-dependent NK cell activation in vitro. (**A**) IFN-γ production of NK cells via polyI:C (pIC)-stimulated DC subsets and Mφs. NK cells, DC subsets, and Mφs were enriched by MACS separation from WT and *Inam*$^{-/-}$ mice. (**B**) Cell-to-cell contact-dependent NK cell activation via CD8α$^+$ cDCs. (**C**) Cell-to-cell contact-dependent NK cell activation via Mφs. NK cells were cocultured with DC subsets and Mφs in the presence of polyI:C (20 μg/ml) for 24 h. The concentrations of IFN-γ in the culture supernatants were measured by ELISA. (**D**) Mφ depletion with clodronate liposomes. WT mice were i.p. injected with clodronate liposomes (150 μl/mouse) to remove Mφs. After 24 h, the efficiency of Mφ depletion was measured by FACS analysis. (**E**) Production of IFN-γ by NK cells in WT, Mφ-depleted WT, and *Batf3*$^{-/-}$ mice. WT, Mφ-depleted WT, and *Batf3*$^{-/-}$ mice were i.p. injected with 200 μg polyI:C ($n = 3$). After 3 h, splenocytes were isolated, cultured with brefeldin A for an additional 4 h, and analyzed for intracellular content of IFN-γ by FACS, gating on CD3ε$^-$/NK1.1$^+$ cells. (**F**) INAM-dependent NK cell activation via CD8α$^+$ cDCs. (**G**) INAM-dependent NK cell activation via Mφs. NK cells, CD8α$^+$ cDCs, and Mφs were enriched via MACS separation from WT and *Inam*$^{-/-}$ mice. NK cells were cocultured with CD8α$^+$ cDCs or Mφs in the presence of polyI:C (20 μg/ml) for 24 h. The concentrations of IFN-γ in the culture supernatants were measured by ELISA. The data shown are representative of at least two independent experiments. Data are means ± SD of three independent samples. *$p < 0.05$.

Downloaded from http://www.jimmunol.org/ at Hokkaido University on February 15, 2015

a result, IFN-γ production was completely blocked under transwell conditions (Fig. 3B, 3C). Therefore, NK cells are primed through contact with CD8α$^+$ cDCs and Mφs independent of soluble mediators. To directly test the contribution of CD8α$^+$ cDCs and Mφs to polyI:C-mediated NK cell activation in vivo, we analyzed *Batf3*$^{-/-}$ mice, which largely lack the CD8α$^+$ cDC population in the spleen of C57BL/6 mice (21), and Mφ-depleted mice generated by clodronate liposome injection (22, 23). Approximately 85% of Mφs were depleted at 24 h after clodronate liposome injection (Fig. 3D). Three hours after polyI:C stimulation, NK cell secretion of IFN-γ was partially decreased in *Batf3*$^{-/-}$ and Mφ-depleted mice (Fig. 3E). These results indicate that CD8α$^+$ cDCs and Mφs are responsible for secretion of IFN-γ from NK cells in response to polyI:C stimulation.

INAM acts on NK cells and BMDC to orchestrate NK–DC interaction triggered by polyI:C stimulation (16). To investigate the role of INAM in the interaction of NK-CD8α$^+$ cDC and NK-Mφ, we performed an experiment on a coculture of MACS-sorted splenic NK cells with their accessory cells isolated from WT and *Inam*$^{-/-}$ mice. Cocultures of NK cells and accessory cells lacking INAM showed that IFN-γ production from NK cells required INAM expression in either NK cells or accessory cells (Fig. 3F, 3G). Notably, deficiency of INAM in both NK and accessory cells led to a marked decrease in IFN-γ production. Taken together, these results suggest that INAM is required for cell–cell contact in both NK cells and accessory cells and early IFN-γ production by NK cells.

INAM plays a critical role in rapid IFN-γ production by NK cells in response to polyI:C in vivo

To investigate the role of INAM in polyI:C-mediated cytotoxicity of NK cells, we injected WT and *Inam*$^{-/-}$ mice with polyI:C. After 0, 3, and 24 h, we isolated splenic NK cells and measured cytotoxicity ex vivo. In the four NK-sensitive cell lines B16D8, RMA-S, B16F10, and YAC-1, we found no difference between WT and *Inam*$^{-/-}$ mice in the cytotoxic effect of NK cells against these cell lines (data not shown). Consistent with these results, cell numbers expressing granzyme B, known as a cytotoxic lymphocyte protease, barely differed between splenocytes of WT and *Inam*$^{-/-}$ mice (Fig. 4A). To determine the role of INAM in NK cell production of IFN-γ in response to polyI:C, we isolated splenocytes 0, 1, and 3 h after injecting WT and *Inam*$^{-/-}$ mice with polyI:C and determined the intracellular content of IFN-γ in NK cells. After 3 h, NK cells isolated from *Inam*$^{-/-}$ mice produced less IFN-γ than WT NK cells (Fig. 4B). Additionally, we also measured the numbers of other cytokine-producing cells, including GM-CSF, IL-2, and TNF-α, from NK cells at 3 h after polyI:C stimulation in WT and *Inam*$^{-/-}$ mice and confirmed no INAM dependence of the production of these cytokines (Supplemental Fig. 2A). Therefore, INAM specifically regulates IFN-γ through CD8α DC at least within this time frame. We also measured CD69 expression, known as an NK-activating marker at 0, 3, and 24 h after polyI:C stimulation. CD69 upregulation in response to polyI:C was partially impaired in NK cells from *Inam*$^{-/-}$ mice in comparison with those from WT mice 24 h after polyI:C stimulation (Fig. 4C). We found no clear difference between WT and *Inam*$^{-/-}$ mice in expression of CD27 or NK1.1, both of which evoke IFN-γ production through their interaction with the ligands, or in any other NK receptors at 0, 3, and 24 h after polyI:C injection (24) (Supplemental Fig. 1B). These results indicate that INAM-mediated NK activation is independent of incremental expression of these receptors. Previous reports suggested that proinflammatory cytokines including IL-12, IL-15, IL-18, and type I IFN play critical roles in the cytotoxicity and IFN-γ production of NK cells (15, 25, 26). To determine their expression at 0, 3, and 24 h

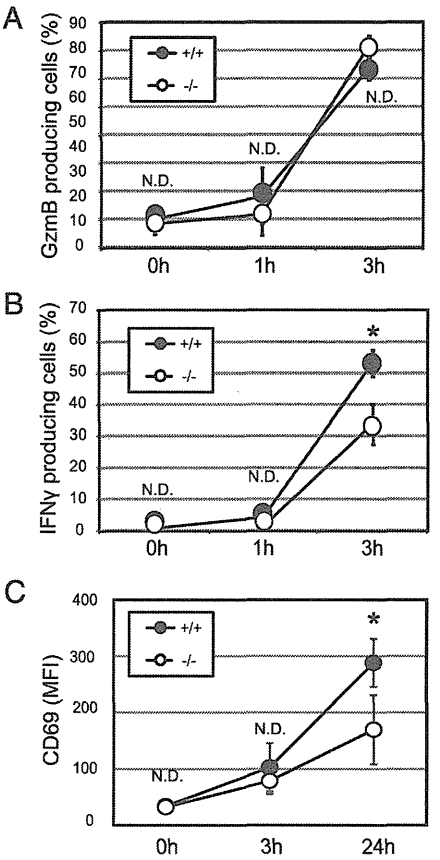

FIGURE 4. INAM-dependent NK cell activation in vivo. (**A**) Production of granzyme B (GzmB) by NK cells. (**B**) Production of IFN-γ by NK cells. WT (+/+) and *Inam*$^{-/-}$ (−/−) mice were i.p. injected with 200 μg polyI:C. After 0, 1, and 3 h, splenocytes were isolated, cultured with brefeldin A for an additional 4 h, and analyzed for intracellular content of IFN-γ and granzyme B by FACS, gating on CD3ε$^-$/NK1.1$^+$ cells (n = 3 or 4). (**C**) Expression of CD69 on the surface of NK cells. WT (+/+) and *Inam*$^{-/-}$ (−/−) mice were i.p. injected with 200 μg polyI:C or PBS. After 0, 3, and 24 h, CD69 expression was assayed by FACS, and the data were quantitatively analyzed using mean fluorescence intensity (MFI), gating on CD3ε$^-$/NK1.1$^+$ cells (n = 3). The data shown are representative of at least two independent experiments. Data are means ± SD of three independent samples. *$p < 0.05$.

after polyI:C stimulation, we performed ELISA and qPCR analysis of serum and spleen cells from WT and *Inam*$^{-/-}$ mice. However, protein levels of IL12p40, IFN-α, and IFN-β were not affected by *Inam* disruption in mice (Supplemental Fig. 2B). Additionally, mRNA expression of *Il-15* and *Il-18* genes was not decreased in *Inam*$^{-/-}$ mice (Supplemental Fig. 2C). These results suggest that INAM plays a critical role in the CD69 expression and rapid IFN-γ production, but not the cytotoxicity, of NK cells in response to polyI:C in a cytokine-independent manner.

INAM is required for the antimetastatic effect by polyI:C-based cancer immunotherapy

Malignant melanomas are one of the most important targets of NK-mediated cancer immunotherapy (27). In this study, we tested two types of polyI:C-based cancer immunotherapy model using B16D8 and B16F10 cell lines. NK cells show high cytotoxicity activity against B16D8 cells established in our laboratory as a subline of the B16 melanoma cell line (28). This subline was characterized by its low or virtually absent metastatic properties when injected s.c. into syngeneic C57BL/6 mice. In contrast, the B16F10 subline was characterized by its high metastatic capacity

Downloaded from http://www.jimmunol.org/ at Hokkaido University on February 15, 2015

especially into the lung (29). In this model, NK1.1$^+$ cells and IFN-γ have a critical role in the suppression of pulmonary metastases (30).

A mouse model with s.c.-implanted B16D8 and polyI:C therapy has been established in our laboratory (8). To investigate the function of INAM involved in tumor growth retardation mediated by polyI:C, we challenged WT and *Inam*$^{-/-}$ mice with B16D8 implantation and then treated the mice with i.p. injection of polyI:C. The rate of B16D8 growth retardation was indistinguishable between WT and *Inam*$^{-/-}$ mice (Supplemental Fig. 3), which was largely dependent on the antitumor effect of polyI:C. This result is consistent with the observation that there is no difference in tumoricidal activity against B16D8 between WT and *Inam*$^{-/-}$ mice. To determine the role of INAM in the production of IFN-γ by lung NK cells in response to polyI:C, we isolated leukocytes from the lung at 0, 3, and 6 h after administration of polyI:C to B16F10-injected WT and *Inam*$^{-/-}$ mice and determined the intracellular content of IFN-γ in NK cells (Fig. 5A). After 6 h, NK cells isolated from *Inam*$^{-/-}$ mice produced less IFN-γ than WT NK cells (Fig. 5B). To investigate the function of INAM involved in pulmonary metastases induced by polyI:C, we i.v. challenged WT and *Inam*$^{-/-}$ mice with B16F10 cells and then treated the mice by i.p. injection of polyI:C. After four rounds of polyI:C treatment, we counted tumor foci in the lung. Under unstimulated conditions, there was no difference in the number and size of tumor foci in the lungs between WT and *Inam*$^{-/-}$ mice (Fig. 5C). In WT mice, i.p. injection of polyI:C exerted a significant inhibition in the growth of pulmonary metastases in tumor-bearing mice compared with PBS controls (Fig. 5D). In contrast, the effect of polyI:C therapy for pulmonary metastases was partially abrogated in *Inam*$^{-/-}$ mice. These results demonstrate that INAM plays a critical role in IFN-γ production by lung NK cells in response to polyI:C and unequivocally exhibits antitumor function in polyI:C-based cancer immunotherapy against IFN-γ–sensitive tumors metastasized to the lung.

BMDC confer direct cytotoxic activity on NK cells by stimulation with RNA via INAM-dependent cell–cell contact (16). Then, NK cells kill tumor cells via effectors, such as TRAIL and granzyme B, secondary to upregulation of INAM. However, splenic DCs hardly induce direct NK cytotoxicity as shown in this study. In this study, *Inam*$^{-/-}$ mice studies revealed that DC/Mφ primed NK cells in vivo to induce IFN-γ that was a major effector for NK antimetastatic activity. Thus, taken together with the previous results that BMDCs induce NK cytotoxicity via INAM (16), INAM-involved DC–NK contact induces two arrays of NK tumoricidal activities, killer effector and IFN-γ producer, depending on the properties of DC subsets. The role of INAM in ILC activation will be a matter of future interest in this context.

Discussion

In this study, we provide the first demonstration, to our knowledge, that INAM plays a critical role in the interactions of NK-CD8α$^+$ cDCs and Mφs leading to IFN-γ production from NK cells in vivo. Additionally, we also propose that INAM is a novel target molecule for cancer immunotherapy against IFN-γ–suppressible metastasis.

IFN-γ coordinates a diverse array of cellular programs via STAT1 activation, such as antimicrobial response, anti- or protumor response, production of proinflammatory cytokines, and induction of IRF1 (31). IRF1 activates a large number of secondary response genes, which carry out a range of immunomodulatory functions (32, 33). In secondary lymphoid organs including spleen and lymph nodes, NK cells are a dominant IFN-γ producer responding to polyI:C (5). IFN-γ primes Ag-specific CD4$^+$ and CD8$^+$ T cells and also activates other innate immune cells including Mφs (34–36). The TLR3-dependent IFN-γ signaling pathway is important in protecting the host from pathogenesis induced by Coxsackievirus group B serotype 3 infection, which leads to IFN-γ production from NK cells (37, 38). Hence, IFN-γ

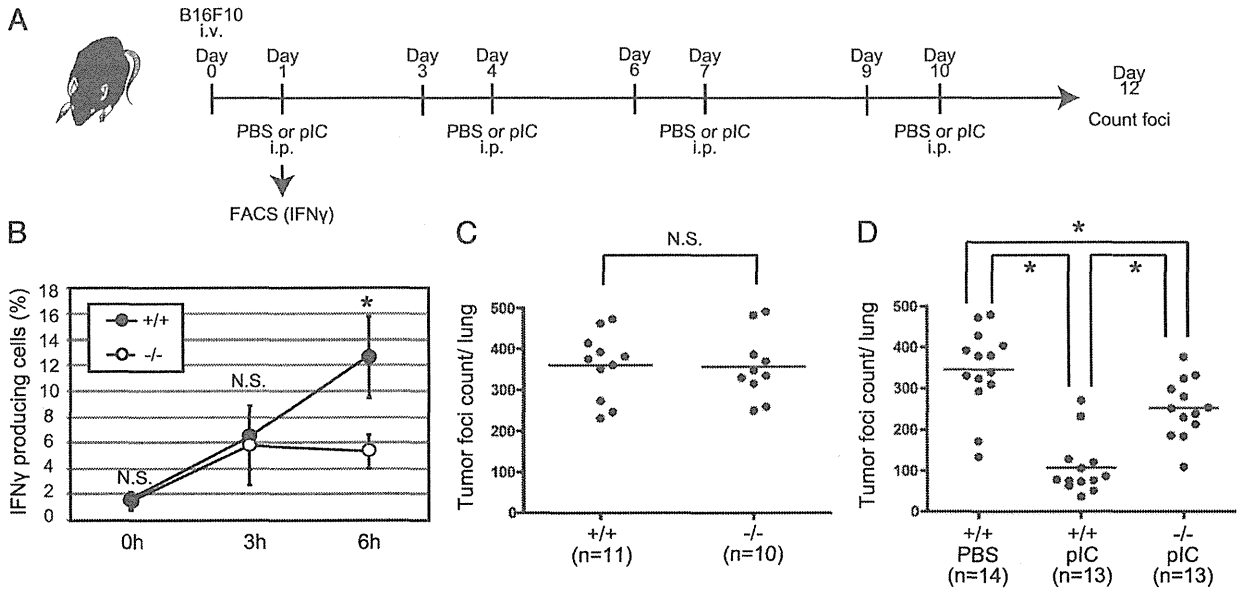

FIGURE 5. Antimetastatic activity of INAM against B16F10 melanoma. (**A**) The time schedule of polyI:C (pIC) treatment. (**B**) Production of IFN-γ by NK cells in the lung. After 24 h, WT and *Inam*$^{-/-}$ mice were i.p. injected with 200 μg polyI:C. Lung leukocytes were isolated and cultured with brefeldin A for an additional 4 h, and analyzed for frequency of NK cells and production of IFN-γ/granzyme B by FACS, gating on CD3ε$^-$/NK1.1$^+$ cells ($n = 3$ or 4). (**C**) Tumor foci counts in the lung of WT (+/+) and *Inam*$^{-/-}$ (−/−) mice under unstimulated conditions at day 12. (**D**) Tumor foci in the lung of WT (+/+) and *Inam*$^{-/-}$ (−/−) mice. WT (+/+) and *Inam*$^{-/-}$ (−/−) mice were i.v. injected with 2×10^5 B16F10 melanoma cells at day 0. At days 1, 4, 7, and 10, WT and *Inam*$^{-/-}$ mice were i.p. injected with 200 μg polyI:C. At day 12, the mice were sacrificed, and lungs were removed and fixed in 10% formalin solution to count surface colonies under a dissection microscope. The data shown are representative of at least two independent experiments. Data are means ± SD of three independent samples. *$p < 0.05$.

Downloaded from http://www.jimmunol.org/ at Hokkaido University on February 15, 2015

derived from NK cells controls innate and adaptive immunity, leading to a Th1 response.

In this study, we show that INAM evokes IFN-γ production by NK cells in the early phase by polyI:C stimulation (Figs. 4B, 5B). In a murine CMV infection model, IFN-γ is induced in NK cells by IL-12 and IL-18 produced by murine CMV–infected CD11b$^+$ cDCs, whereas these cytokines barely evoke any cytotoxic response in NK cells (39). In addition, IFN-γ production from NK cells is induced by anti-CD27 Ab stimulation, but again no cytotoxic response is triggered (24). Therefore, these reports indicate that NK cell cytotoxicity and IFN-γ production are independently controlled by different mechanisms. We found no clear difference between WT and *Inam*$^{-/-}$ mice in expression of these cell surface molecules and cytokines. Hence, the INAM-dependent IFN-γ production from NK cells is based on an as-yet-unknown mechanism(s) acting in a manner independent of these molecules.

CpG DNA is known to induce IFN-γ from NK cells, which is mediated through pDCs. TLR9 in pDCs responds to CpG, and the pDCs liberate IFN-α and TNF-α that participate in the induction of IFN-γ from NK cells (40). We checked induction of the Inam mRNA in spleen after stimulation with CpG in WT and *Inam*$^{-/-}$ mice (Fig. 1E). The levels of *Inam* mRNA as well as numbers of IFN-γ–producing cells were hardly increased in response to i.p. administration of CpG in WT as well as *Inam*$^{-/-}$ mice, suggesting no participation of INAM in CpG-induced NK cell IFN-γ production (data not shown). CpG participates in the activation of the TLR9 pathway in pDCs, but INAM in splenic cDCs and Mφs does not participate in CpG-mediated NK priming. The result is consistent with the fact that polyI:C is an agonist for TLR3 (but not for TLR9 predominantly expressed in pDCs), which is mainly expressed in CD8α$^+$ DCs, especially professional Ag-presenting CD141$^+$ and CD103$^+$ DCs in mice (41).

CD8α$^+$ cDCs directly recognize polyI:C via the TLR3/TICAM-1 pathway and promote IFN-γ production from NK cells in vitro (9). However, previous analysis of *Batf3*$^{-/-}$ mice indicated that absence of CD8α$^+$ cDCs resulted in weak NK cell activation, in agreement with our data (19). We also found that NK cell secretion of IFN-γ was partially decreased in mice depleted of Mφs by injection of clodronate liposomes (Fig. 3E). Notably, expression of INAM by both NK cells and accessory cells is required for early IFN-γ production through NK-CD8α$^+$ cDC and/or NK–Mφ interactions (Fig. 3F, 3G). The physiological role of these accessory cells in NK activation is poorly understood. However, our results indicate that CD8α$^+$ cDCs and Mφs facilitate early secretion of IFN-γ from NK cells in response to polyI:C and INAM plays a critical role in the interaction between NK cells and CD8α$^+$ cDCs and/or Mφs, leading to IFN-γ production.

IFN-γ exhibits both anti- and protumor activities (42). Systemic administration of polyI:C exerted a significant inhibitory effect on the growth of lung metastases in B16F10 melanoma-bearing mice (30, 42). Using this model, a previous study reported that NK1.1$^+$ cells and IFN-γ have a critical role in the protection of lung metastases (30). Previous studies demonstrated that the IFN-γ receptor expressed on host cells, but not on melanoma cells, is important for development of lung metastases (43–45). Hence, lung metastases are prevented by the IFN-γ–inducible immune response following NK cell activation. We show that INAM is involved in the IFN-γ production of lung NK cells in response to polyI:C stimulation and unequivocally exhibits antitumor functions in polyI:C-based cancer immunotherapy against IFN-γ–sensitive tumor foci in the lung (Fig. 5D). Therefore, we propose that INAM is a novel target molecule for cancer immunotherapy against IFN-γ–suppressible metastasis.

Acknowledgments

We thank the members in Seya Laboratory (Hokkaido University). Tumor implant studies were supported by A. Morii-Sakai (Seya Laboratory). Thoughtful discussions with Dr. T. Taniguchi (University of Tokyo) are gratefully acknowledged.

Disclosures

The authors have no financial conflicts of interest.

References

1. Seya, T., J. Kasamatsu, M. Azuma, H. Shime, and M. Matsumoto. 2011. Natural killer cell activation secondary to innate pattern sensing. *J. Innate Immun.* 3: 264–273.
2. Reed, S. G., M. T. Orr, and C. B. Fox. 2013. Key roles of adjuvants in modern vaccines. *Nat. Med.* 19: 1597–1608.
3. Kumar, H., S. Koyama, K. J. Ishii, T. Kawai, and S. Akira. 2008. Cutting edge: cooperation of IPS-1- and TRIF-dependent pathways in poly IC-enhanced antibody production and cytotoxic T cell responses. *J. Immunol.* 180: 683–687.
4. Trumpfheller, C., M. Caskey, G. Nchinda, M. P. Longhi, O. Mizenina, Y. Huang, S. J. Schlesinger, M. Colonna, and R. M. Steinman. 2008. The microbial mimic poly IC induces durable and protective CD4$^+$ T cell immunity together with a dendritic cell targeted vaccine. *Proc. Natl. Acad. Sci. USA* 105: 2574–2579.
5. Longhi, M. P., C. Trumpfheller, J. Idoyaga, M. Caskey, I. Matos, C. Kluger, A. M. Salazar, M. Colonna, and R. M. Steinman. 2009. Dendritic cells require a systemic type I interferon response to mature and induce CD4+ Th1 immunity with poly IC as adjuvant. *J. Exp. Med.* 206: 1589–1602.
6. Talmadge, J. E., J. Adams, H. Phillips, M. Collins, B. Lenz, M. Schneider, E. Schlick, R. Ruffmann, R. H. Wiltrout, and M. A. Chirigos. 1985. Immunomodulatory effects in mice of polyinosinic-polycytidylic acid complexed with poly-L-lysine and carboxymethylcellulose. *Cancer Res.* 45: 1058–1065.
7. Spits, H., D. Artis, M. Colonna, A. Diefenbach, J. P. Di Santo, G. Eberl, S. Koyasu, R. M. Locksley, A. N. McKenzie, R. E. Mebius, et al. 2013. Innate lymphoid cells—a proposal for uniform nomenclature. *Nat. Rev. Immunol.* 13: 145–149.
8. Akazawa, T., T. Ebihara, M. Okuno, Y. Okuda, M. Shingai, K. Tsujimura, T. Takahashi, M. Ikawa, M. Okabe, N. Inoue, et al. 2007. Antitumor NK activation induced by the Toll-like receptor 3-TICAM-1 (TRIF) pathway in myeloid dendritic cells. *Proc. Natl. Acad. Sci. USA* 104: 252–257.
9. Miyake, T., Y. Kumagai, H. Kato, Z. Guo, K. Matsushita, T. Satoh, T. Kawagoe, H. Kumar, M. H. Jang, T. Kawai, et al. 2009. Poly I:C-induced activation of NK cells by CD8 alpha+ dendritic cells via the IPS-1 and TRIF-dependent pathways. *J. Immunol.* 183: 2522–2528.
10. Wulff, S., R. Pries, and B. Wollenberg. 2010. Cytokine release of human NK cells solely triggered with Poly I:C. *Cell. Immunol.* 263: 135–137.
11. Fuchs, A., W. Vermi, J. S. Lee, S. Lonardi, S. Gilfillan, R. D. Newberry, M. Cella, and M. Colonna. 2013. Intraepithelial type 1 innate lymphoid cells are a unique subset of IL-12- and IL-15-responsive IFN-γ-producing cells. *Immunity* 38: 769–781.
12. Matsumoto, M., K. Funami, H. Oshiumi, and T. Seya. 2013. Toll-IL-1-receptor-containing adaptor molecule-1: a signaling adaptor linking innate immunity to adaptive immunity. *Prog. Mol. Biol. Transl. Sci.* 117: 487–510.
13. Shime, H., A. Kojima, A. Maruyama, Y. Saito, H. Oshiumi, M. Matsumoto, and T. Seya. 2014. Myeloid-derived suppressor cells confer tumor-suppressive functions on natural killer cells via polyinosinic:polycytidylic acid treatment in mouse tumor models. *J. Innate Immun.* 6: 293–305.
14. Tu, Z., A. Bozorgzadeh, R. H. Pierce, J. Kurtis, I. N. Crispe, and M. S. Orloff. 2008. TLR-dependent cross talk between human Kupffer cells and NK cells. *J. Exp. Med.* 205: 233–244.
15. Lucas, M., W. Schachterle, K. Oberle, P. Aichele, and A. Diefenbach. 2007. Dendritic cells prime natural killer cells by trans-presenting interleukin 15. *Immunity* 26: 503–517.
16. Ebihara, T., M. Azuma, H. Oshiumi, J. Kasamatsu, K. Iwabuchi, K. Matsumoto, H. Saito, T. Taniguchi, M. Matsumoto, and T. Seya. 2010. Identification of a polyI:C-inducible membrane protein that participates in dendritic cell-mediated natural killer cell activation. *J. Exp. Med.* 207: 2675–2687.
17. Sato, M., H. Suemori, N. Hata, M. Asagiri, K. Ogasawara, K. Nakao, T. Nakaya, M. Katsuki, S. Noguchi, N. Tanaka, and T. Taniguchi. 2000. Distinct and essential roles of transcription factors IRF-3 and IRF-7 in response to viruses for IFN-alpha/beta gene induction. *Immunity* 13: 539–548.
18. Takaki, H., M. Takeda, M. Tahara, M. Shingai, H. Oshiumi, M. Matsumoto, and T. Seya. 2013. The MyD88 pathway in plasmacytoid and CD4+ dendritic cells primarily triggers type I IFN production against measles virus in a mouse infection model. *J. Immunol.* 191: 4740–4747.
19. McCartney, S., W. Vermi, S. Gilfillan, M. Cella, T. L. Murphy, R. D. Schreiber, K. M. Murphy, and M. Colonna. 2009. Distinct and complementary functions of MDA5 and TLR3 in poly(I:C)-mediated activation of mouse NK cells. *J. Exp. Med.* 206: 2967–2976.
20. Hayakawa, Y., N. D. Huntington, S. L. Nutt, and M. J. Smyth. 2006. Functional subsets of mouse natural killer cells. *Immunol. Rev.* 214: 47–55.
21. Edelson, B. T., T. R. Bradstreet, W. Kc, K. Hildner, J. W. Herzog, J. Sim, J. H. Russell, T. L. Murphy, E. R. Unanue, and K. M. Murphy. 2011. Batf3-dependent CD11b(low/-) peripheral dendritic cells are GM-CSF-independent

Downloaded from http://www.jimmunol.org/ at Hokkaido University on February 15, 2015

and are not required for Th cell priming after subcutaneous immunization. *PLoS ONE* 6: e25660.
22. Hildner, K., B. T. Edelson, W. E. Purtha, M. Diamond, H. Matsushita, M. Kohyama, B. Calderon, B. U. Schraml, E. R. Unanue, M. S. Diamond, et al. 2008. Batf3 deficiency reveals a critical role for CD8alpha$^+$ dendritic cells in cytotoxic T cell immunity. *Science* 322: 1097–1100.
23. Tussiwand, R., W. L. Lee, T. L. Murphy, M. Mashayekhi, W. Kc, J. C. Albring, A. T. Satpathy, J. A. Rotondo, B. T. Edelson, N. M. Kretzer, et al. 2012. Compensatory dendritic cell development mediated by BATF-IRF interactions. *Nature* 490: 502–507.
24. Takeda, K., H. Oshima, Y. Hayakawa, H. Akiba, M. Atsuta, T. Kobata, K. Kobayashi, M. Ito, H. Yagita, and K. Okumura. 2000. CD27-mediated activation of murine NK cells. *J. Immunol.* 164: 1741–1745.
25. Ferlazzo, G., M. Pack, D. Thomas, C. Paludan, D. Schmid, T. Strowig, G. Bougras, W. A. Muller, L. Moretta, and C. Münz. 2004. Distinct roles of IL-12 and IL-15 in human natural killer cell activation by dendritic cells from secondary lymphoid organs. *Proc. Natl. Acad. Sci. USA* 101: 16606–16611.
26. Takeda, K., H. Tsutsui, T. Yoshimoto, O. Adachi, N. Yoshida, T. Kishimoto, H. Okamura, K. Nakanishi, and S. Akira. 1998. Defective NK cell activity and Th1 response in IL-18-deficient mice. *Immunity* 8: 383–390.
27. Burke, S., T. Lakshmikanth, F. Colucci, and E. Carbone. 2010. New views on natural killer cell-based immunotherapy for melanoma treatment. *Trends Immunol.* 31: 339–345.
28. Tanaka, H., Y. Mori, H. Ishii, and H. Akedo. 1988. Enhancement of metastatic capacity of fibroblast-tumor cell interaction in mice. *Cancer Res.* 48: 1456–1459.
29. Brown, L. M., D. R. Welch, and S. R. Rannels. 2002. B16F10 melanoma cell colonization of mouse lung is enhanced by partial pneumonectomy. *Clin. Exp. Metastasis* 19: 369–376.
30. Jiang, Q., H. Wei, and Z. Tian. 2008. IFN-producing killer dendritic cells contribute to the inhibitory effect of poly I:C on the progression of murine melanoma. *J. Immunother.* 31: 555–562.
31. Schroder, K., P. J. Hertzog, T. Ravasi, and D. A. Hume. 2004. Interferon-gamma: an overview of signals, mechanisms and functions. *J. Leukoc. Biol.* 75: 163–189.
32. Honda, K., and T. Taniguchi. 2006. IRFs: master regulators of signalling by Toll-like receptors and cytosolic pattern-recognition receptors. *Nat. Rev. Immunol.* 6: 644–658.
33. Miyamoto, M., T. Fujita, Y. Kimura, M. Maruyama, H. Harada, Y. Sudo, T. Miyata, and T. Taniguchi. 1988. Regulated expression of a gene encoding a nuclear factor, IRF-1, that specifically binds to IFN-beta gene regulatory elements. *Cell* 54: 903–913.
34. O'Sullivan, T., R. Saddawi-Konefka, W. Vermi, C. M. Koebel, C. Arthur, J. M. White, R. Uppaluri, D. M. Andrews, S. F. Ngiow, M. W. L. Teng, et al. 2012. Cancer immunoediting by the innate immune system in the absence of adaptive immunity. *J. Exp. Med.* 209: 1869–1882.
35. Mailliard, R. B., Y. I. Son, R. Redlinger, P. T. Coates, A. Giermasz, P. A. Morel, W. J. Storkus, and P. Kalinski. 2003. Dendritic cells mediate NK cell help for Th1 and CTL responses: two-signal requirement for the induction of NK cell helper function. *J. Immunol.* 171: 2366–2373.
36. Martín-Fontecha, A., L. L. Thomsen, S. Brett, C. Gerard, M. Lipp, A. Lanzavecchia, and F. Sallusto. 2004. Induced recruitment of NK cells to lymph nodes provides IFN-gamma for T(H)1 priming. *Nat. Immunol.* 5: 1260–1265.
37. Hühn, M. H., M. Hultcrantz, K. Lind, H. G. Ljunggren, K. J. Malmberg, and M. Flodström-Tullberg. 2008. IFN-gamma production dominates the early human natural killer cell response to Coxsackievirus infection. *Cell. Microbiol.* 10: 426–436.
38. Negishi, H., T. Osawa, K. Ogami, X. Ouyang, S. Sakaguchi, R. Koshiba, H. Yanai, Y. Seko, H. Shitara, K. Bishop, et al. 2008. A critical link between Toll-like receptor 3 and type II interferon signaling pathways in antiviral innate immunity. *Proc. Natl. Acad. Sci. USA* 105: 20446–20451.
39. Andoniou, C. E., S. L. H. van Dommelen, V. Voigt, D. M. Andrews, G. Brizard, C. Asselin-Paturel, T. Delale, K. J. Stacey, G. Trinchieri, and M. A. Degli-Esposti. 2005. Interaction between conventional dendritic cells and natural killer cells is integral to the activation of effective antiviral immunity. *Nat. Immunol.* 6: 1011–1019.
40. Marshall, J. D., D. S. Heeke, C. Abbate, P. Yee, and G. Van Nest. 2006. Induction of interferon-gamma from natural killer cells by immunostimulatory CpG DNA is mediated through plasmacytoid-dendritic-cell-produced interferon-alpha and tumour necrosis factor-alpha. *Immunology* 117: 38–46.
41. Jongbloed, S. L., A. J. Kassianos, K. J. McDonald, G. J. Clark, X. Ju, C. E. Angel, C. J. Chen, P. R. Dunbar, R. B. Wadley, V. Jeet, et al. 2010. Human CD141+ (BDCA-3)+ dendritic cells (DCs) represent a unique myeloid DC subset that cross-presents necrotic cell antigens. *J. Exp. Med.* 207: 1247–1260.
42. Zaidi, M. R., and G. Merlino. 2011. The two faces of interferon-γ in cancer. *Clin. Cancer Res.* 17: 6118–6124.
43. Forte, G., A. Rega, S. Morello, A. Luciano, C. Arra, A. Pinto, and R. Sorrentino. 2012. Polyinosinic-polycytidylic acid limits tumor outgrowth in a mouse model of metastatic lung cancer. *J. Immunol.* 188: 5357–5364.
44. Takeda, K., M. Nakayama, M. Sakaki, Y. Hayakawa, M. Imawari, K. Ogasawara, K. Okumura, and M. J. Smyth. 2011. IFN-γ production by lung NK cells is critical for the natural resistance to pulmonary metastasis of B16 melanoma in mice. *J. Leukoc. Biol.* 90: 777–785.
45. Kakuta, S., Y. Tagawa, S. Shibata, M. Nanno, and Y. Iwakura. 2002. Inhibition of B16 melanoma experimental metastasis by interferon-gamma through direct inhibition of cell proliferation and activation of antitumour host mechanisms. *Immunology* 105: 92–100.

Downloaded from http://www.jimmunol.org/ at Hokkaido University on February 15, 2015

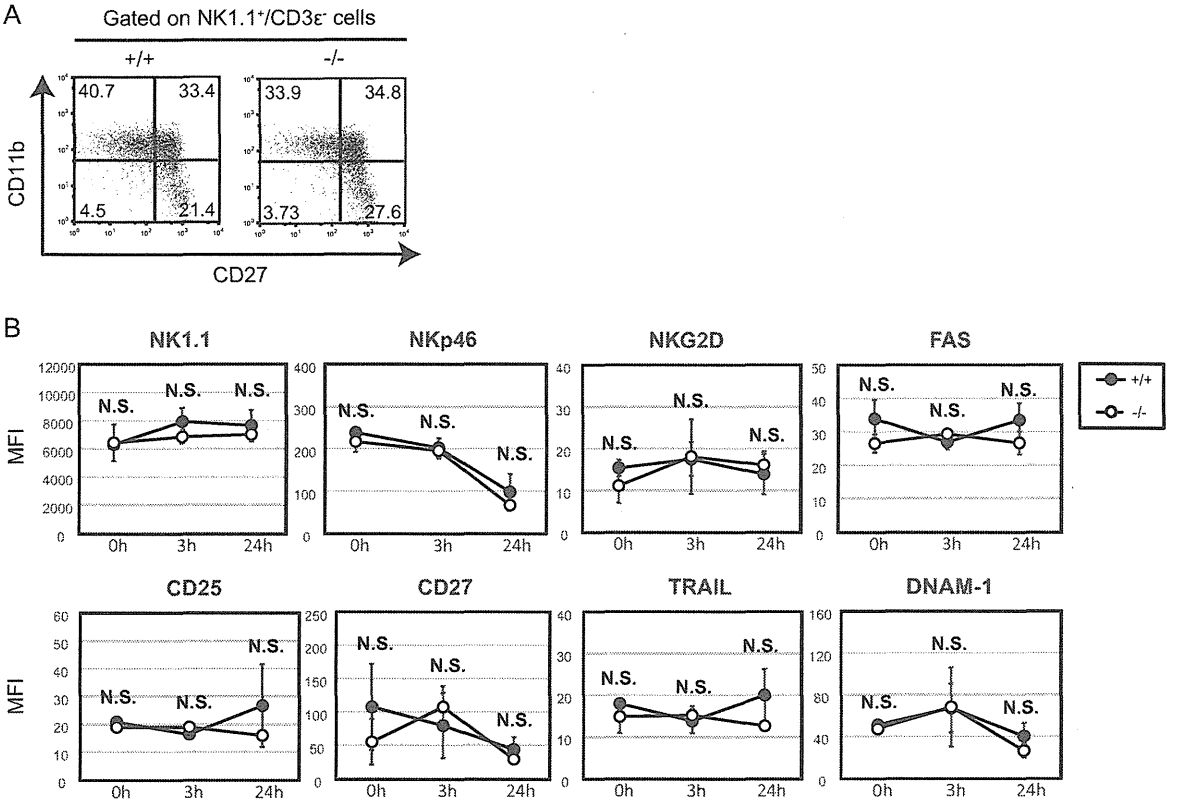

Supplementary Figure 1. Development and NK receptors/effector molecules of NK cells in WT and *Inam*$^{-/-}$ mice.

(A) Development of NK cells in WT and *Inam*$^{-/-}$ mice. Flow cytometric analysis of CD27/CD11b expression by splenic NK cells in WT (+/+) and Inam$^{-/-}$ (−/−) mice (n = 2). (B) Expression of NK receptors and activating/effector molecules on NK cells in WT and *Inam*$^{-/-}$ mice. WT (+/+) and *Inam*$^{-/-}$ (−/−) mice were injected intraperitoneally with 200 μg polyI:C or PBS. After 0h, 3h and 24h, expression of NK receptors/ effector molecules on NK cells was assayed by FACS, gating on CD3ε-/NK1.1+ cells except for NK1.1 expression (n = 3). For NK1.1 expression, CD3ε-/NKp46+ cells were assayed by FACS. The data shown are representative of at least two independent experiments. Data are means ± SD of three independent samples. *p < 0.05.